Atmos. Chem. Phys. Discuss., 12, 23913–23974, 2012
www.atmos-chem-phys-discuss.net/12/23913/2012/
doi:10.5194/acpd-12-23913-2012

Atmospheric Chemistry and Physics Discussions

An empirical model of global climate – Part 2: Implications for future temperature

N. R. Mascioli[1], **T. Canty**[1], **and R. J. Salawitch**[1,2,3]

[1]Department of Atmospheric and Oceanic Science, University of Maryland, College Park, MD, USA
[2]Department of Chemistry and Biochemistry, University of Maryland, College Park, MD, USA
[3]Earth System Science Interdisciplinary Center, University of Maryland, College Park, MD, USA

Received: 27 July 2012 – Accepted: 28 August 2012 – Published: 13 September 2012

Correspondence to: R. J. Salawitch (rjs@atmos.umd.edu)

Published by Copernicus Publications on behalf of the European Geosciences Union.

Abstract

IPCC (2007) has shown that atmosphere-ocean general circulation models (GCMs) from various research centers simulate the rise in global mean surface temperature over the past century rather well, yet provide divergent estimates of temperature for the upcoming decades. We use an empirical model of global climate based on a multiple linear regression (MLR) analysis of the past global surface temperature anomalies (ΔT) to explore why GCMs might provide divergent estimates of future temperature. Our focus is on the interplay of three factors: net anthropogenic aerosol radiative forcing (NAA RF), climate feedback (water vapor, clouds, surface albedo) in response to greenhouse gas radiative forcing (GHG RF), and ocean heat export (OHE). Our model is predicated on two key assumptions: whatever climate feedback is needed to account for past temperature rise will persist into the future and whatever fraction of anthropogenic RF (GHG RF + NAA RF) is exported to the oceans to match the observed rise in ocean heat content will also persist. Even with these assumptions, modeled future ΔT mimics the behavior of GCMs because the ~110 record of global surface temperature can not distinguish between two possibilities. If anthropogenic aerosols presently exert small cooling on global climate, feedback must be weak and the future rise in global average surface temperature in 2053, the time CO_2 is projected to double according to RCP 8.5, could be moderate. If aerosols presently exert large cooling of global climate, feedback must be large and future ΔT when CO_2 doubles could be substantial. Reduced uncertainty for climate projection requires observationally based constraints that can narrow the uncertainties that presently exist for net anthropogenic aerosol radiative forcing as well as the totality of feedbacks that occur in response to a GHG RF perturbation. GCMs are often compared by evaluating the equilibrium response to a doubling of CO_2, termed climate sensitivity. In our model framework, ΔT at the time CO_2 doubles is nearly independent of OHE, because climate feedback must be adjusted to properly simulate observed temperature. Our simulations show that if a small fraction of anthropogenic RF is exported to the ocean, equilibrium climate

ACPD

12, 23913–23974, 2012

sensitivity closely represents the modeled ΔT at the time CO_2 doubles. Conversely, if this fraction is large, ΔT when CO_2 doubles is much less than the equilibrium climate sensitivity (i.e. the model is now far from equilibrium). Similar behavior likely occurs within GCMs. We therefore suggest the dependence of climate sensitivity on OHE be factored into analyses that use this metric to compare and evaluate GCMs.

1 Introduction

Atmosphere and ocean general circulation models (GCMs) driven by prescribed abundances of greenhouse gases (GHGs) provide reasonably good simulations of global mean surface temperature over the past century (e.g. Fig. 9.5a of IPCC, 2007) yet diverge when projecting future temperature (e.g. Fig. 10.5 of IPCC, 2007 and Fig. 1 of Knutti et al., 2010). The divergence of future climate simulations provided by GCMs is often cast in terms of $\Delta T_{2\times CO_2}$, the rise in equilibrium global mean surface temperature projected to occur for a doubling of atmospheric CO_2 relative to pre-industrial levels (hereafter, CO_2 doubling). The quantity $\Delta T_{2\times CO_2}$ is commonly called climate sensitivity (e.g. Kiehl, 2007; Schwartz et al., 2007; Knutti and Hegerl, 2008; Knutti et al., 2010). Kiehl (2007) poses the central question of our study: "if climate models differ by a factor of 2 to 3 in their climate sensitivity, how can they all simulate the global temperature record with a reasonable degree of accuracy?"

We use an empirical model of global climate, based on a multiple linear regression (MLR) analysis of the CRU4 global, monthly mean near surface air (hereafter, surface) temperature anomaly (ΔT) from 1900 to 2010 (Morice et al., 2012) coupled with a simple representation of the physics of global warming, to explore the question posed by Kiehl (2007). He addressed this question by examining the relation between net anthropogenic aerosol radiative forcing (NAA RF) and $\Delta T_{2\times CO_2}$ found by nine atmosphere ocean general circulation models (GCMs). Knutti et al. (2002) also examined this question, focusing on the dependence of climate sensitivity on ocean heat export (OHE). Here, we examine the behavior of climate sensitivity in terms of NAA RF and OHE, as

ACPD
12, 23913–23974, 2012

well as the climate feedback that occurs in a response to a GHG radiative forcing (GHG RF) perturbation, represented by our sensitivity parameter γ.

We show, as described by Kiehl (2007), that equally good simulations of past climate can be obtained for various relations of NAA RF and γ. If aerosols have strongly cooled, a good simulation of climate requires large climate feedback (high γ) in response to the GHG perturbation. If aerosols have weakly cooled, a good simulation of climate requires small feedback (low γ). As suggested by Kiehl (2007), we show that the specific NAA RF versus γ relation needed to obtain a good simulation of past ΔT depends on OHE.

Our model exhibits another interesting behavior that could be important for making further progress on the question posed by Kiehl (2007). If OHE is small, a good simulation of climate can be obtained with small feedback because a large fraction of the total anthropogenic radiative forcing (AF) heats the surface and atmosphere. In this case, modeled temperature is close to equilibrium temperature: the computed value of ΔT at the time CO_2 doubles lies close to the model equilibrium climate sensitivity, $\Delta T_{2\times CO_2}$. On the other hand, if OHE is large, a good simulation of past climate requires large feedback because only a small fraction of AF heats the atmosphere: the model is far from equilibrium and ΔT at the time CO_2 doubles is much smaller than $\Delta T_{2\times CO_2}$. We show that future ΔT at the time CO_2 doubles is mainly dependent on γ and NAA RF for the contemporary atmosphere and illustrate why $\Delta T_{2\times CO_2}$ is a complicated diagnostic to use for evaluating climate models.

Projections of globally averaged surface temperature are given for the four Representation Concentration Pathways (RCP) scenarios of future GHG abundance and aerosol precursor emissions prepared for the upcoming IPCC report (Meinshausen et al., 2011; van Vuuren et al., 2011a). These projections are based on the set of values of γ and NAA RF that provide an acceptable fit to the century long ΔT record within our model framework. Our temperature projection agrees quite well with the ensemble mean and spread of simulated future temperature found by GCMs constrained to the Special Report on Emission Scenarios (SRES) A1B scenario used by IPCC (2007) and Rowlands

ACPD
12, 23913–23974, 2012

et al. (2012). Since the calculations shown in our paper can be conducted in an afternoon on a modern work station, a MLR model used as described below could provide a useful complement to ensemble GCM runs that require enormous, community-wide effort.

Section 2 provides an overview of our model. Since the model is described in detail within our companion paper (Canty et al., 2012), we provide below a detailed description of only the most important parameters (GHG RF, NAA RF, OHE, and γ). Section 3 describes the simulations conducted using the model. Section 4 relates our findings to the literature on NAA RF and climate feedback. Section 5 presents our conclusions. Canty et al. (2012) include appendices that describe glossary of terms, web addresses (URLs) of data, calculation of statistical uncertainty of regression coefficients, and the uncertainty in NAA RF. These appendices may be useful to readers of this paper.

2 Empirical model of global climate

Our model framework, multiple linear regression (MLR), is similar to Lean and Rind (2009), except we explicitly represent ocean heat export (OHE). Throughout, radiative forcing (RF) refers to the stratospheric-adjusted RF described in Sect. 2.2 of IPCC (2007). Radiative forcing due to GHGs and net anthropogenic aerosol RF are specified based on GHG abundances and direct aerosol RF terms provided by the RCP database (Meinshausen et al., 2011; van Vuuren et al., 2011a), with one exception, for sulfate aerosols, described in Sect. 2.2.3. We represent total climate feedback that occurs in a response to a GHG RF perturbation by a single term, the sensitivity parameter, γ. Another important model parameter is the fraction of anthropogenic RF (i.e. GHG RF plus NAA RF) that heats the upper ocean, termed Ω.

Lean and Rind (2009) showed a single projection of future temperature based on a best fit regression for a specified time series of NAA RF. They did not explicitly represent OHE. Here, we quantitatively evaluate the impact of uncertainties in NAA RF and OHE on future temperature. Most importantly, rather than relying solely on best fits

ACPD
12, 23913–23974, 2012

from the regression, we use reduced chi-squared as a metric to evaluate the impact on future temperature of the set of acceptable fits.

2.1 Model equations

Our regression model minimizes the following Cost Function:

$$\text{Cost Function} = \sum_{i=1}^{N_{\text{MONTHS}}} \frac{1}{\sigma^2_{\text{OBS } i}} (\Delta T_{\text{OBS } i} - \Delta T_{\text{MDL } i})^2 \quad (1)$$

where $\Delta T_{\text{OBS } i}$ and $\Delta T_{\text{MDL } i}$ represent time series of observed and modeled global, monthly mean surface temperature anomalies, $\sigma_{\text{OBS } i}$ is the 1-sigma uncertainty associated with each temperature observation, and i denotes month. $\Delta T_{\text{MDL } i}$ is expressed as:

$$\Delta T_{\text{MDL } i} = \lambda(1+\gamma)(\text{GHG RF}_i) + \lambda(\text{NAA RF}_i) + C_o + C_1 \times \text{SOD}_{i-6} + C_2 \times \text{TSI}_i + C_3 \times \text{ENSO}_i + C_4 \times \text{AMO}_i + C_5 \times \text{PDO}_i + C_6 \times \text{IOD}_i - \lambda Q_{\text{OCEAN } i} \quad (2)$$

We base $\Delta T_{\text{OBS } i}$ on the global, monthly mean surface temperature anomaly provided by the Climate Research Unit (Morice et al., 2012), as described in Sect. 2.2.1. The term λ in Eq. (2) represents the response of surface temperature to a RF perturbation without consideration of feedbacks, for present day albedo. This term is set to $0.3\,^{\circ}\text{C}/(\text{W m}^{-2})$ throughout (Sect. 3.2 of Canty et al., 2012 and references therein).

We refer to γ as the sensitivity parameter. This term represents the sensitivity of climate to all feedbacks that occur in response to a GHG perturbation to RF. Should one decompose γ into component terms, the inverse of each term would be additive, i.e.:

$$\frac{1}{\gamma} = \frac{1}{\gamma_{\text{WATER VAPOR}}} + \frac{1}{\gamma_{\text{LAPSE RATE}}} + \frac{1}{\gamma_{\text{SURFACE ALBEDO}}} + \frac{1}{\gamma_{\text{CLOUDS}}} \quad (3)$$

ACPD
12, 23913–23974, 2012

(e.g. Eq. 12 of Hansen et al., 1984). The sensitivity parameter is central to our analysis and many figures either show results as a function of γ or else denote the best fit value of γ found from a regression. This parameter is discussed in greater detail within Sect. 3.2 of Canty et al. (2012).

There are also important climate feedbacks involving tropospheric aerosols (e.g. Fig. 2.10 of IPCC, 2007). Aerosol feedbacks are implicit in the scaling terms used to define NAA RF_i, which represents global, monthly mean total RF due to all anthropogenic aerosols *including feedbacks*. It is essential that the sensitivity of climate to a GHG perturbation (parameter γ) and tropospheric aerosols be treated independently because the physical processes that link perturbation to response are extremely different for GHGs and aerosols. In addition, the forcing of global climate due to tropospheric aerosols is projected to greatly diminish over the next half-century (Riahi et al., 2007, 2011; Matthews and Zickfeld, 2012).

The export of heat from the atmosphere to the ocean is represented by:

$$Q_{\mathrm{OCEAN}\ i} = \Omega[(1+\gamma)\,\mathrm{GHG\ RF}_{i-72} + \mathrm{NAA\ RF}_{i-72}] \tag{4}$$

where

$$\Omega = \frac{\mathrm{OHE}}{\langle(1+\gamma)\mathrm{GHG\ RF} + \mathrm{NAA\ RF}\rangle_{\mathrm{TIME\ INITIAL\ TO\ TIME\ FINAL}}} \tag{5}$$

The index $i - 72$ in Eq. (4) represents the 6 yr (72 month) lag between an atmospheric RF perturbation and heat export to the upper ocean (Schwartz, 2012). The term OHE in Eq. (5) represents the rise in ocean heat content (OHC) over the period of observation. The notation $\langle\ \rangle_{\mathrm{TIME\ INITIAL\ to\ TIME\ FINAL}}$ denotes the mean value of the term enclosed within brackets over the specified time period.

Equations (4) and (5) are designed to represent our simple approach for handling ocean heat export. Equation (5) is used to determine Ω, the fraction of anthropogenic RF perturbation to climate (AF) exported to the ocean over the time period of OHC observation. Equation (4) represents our assumption that the same fraction of AF is

ACPD
12, 23913–23974, 2012

exported to the ocean for other times, either past or future, when OHC observations are not available. A more sophisticated approach would use heat uptake coefficients to drive atmosphere to ocean heat transfer, based on thermal gradients between the atmosphere and ocean (e.g. Schwartz, 2012). If the transfer of heat from the atmosphere to ocean is indeed proportional to thermal gradients between various compartments of the climate system, and if ΔT is linearly proportional to AF (as commonly assumed in models of this nature), then the approach represented by Eqs. (4) and (5) provides an accurate representation of the physical process that drives OHE.

As detailed in Sect. 3.2.4 of Canty et al. (2012), for the Church et al. (2011) measurement of OHC, Eq. (5) becomes:

$$\Omega = \frac{0.347\ \mathrm{W\ m^{-2}}}{\langle (1+\gamma)\mathrm{GHG\ RF} + \mathrm{NAA\ RF}\rangle_{1944\ \mathrm{to}\ 2003}} \tag{6}$$

If the Gouretski and Reseghetti (2010) measurement of OHC is used instead, Eq. (5) becomes:

$$\Omega = \frac{1.22\ \mathrm{W\ m^{-2}}}{\langle (1+\gamma)\mathrm{GHG\ RF} + \mathrm{NAA\ RF}\rangle_{1987\ \mathrm{to}\ 2002}} \tag{7}$$

Past and future time series of radiative forcing due to greenhouse gases (GHG RF_i) and net anthropogenic aerosols (NAA RF_i) are tied to the RCP database (Meinshausen et al., 2011; van Vuuren et al., 2011a), as explained in Sects. 2.2.2 and 2.2.3. As described in Sect. 2.2.3, scaling parameters α_{COOL} and α_{HEAT} are used to convert estimates of direct RF from "aerosols that cool" (mainly sulfate) and "aerosols that heat" (mainly black carbon) into NAA RF.

The regression model also includes proxies that represent the influence on ΔT of variations in total solar irradiance (TSI), stratospheric optical depth (SOD) due mainly to volcanoes, as well as internal variability in ocean circulation represented by El Niño-Southern Oscillation (ENSO), the Atlantic Multidecadal Oscillation (AMO), the Pacific Decadal Oscillation (PDO), and the Indian Ocean Dipole (IOD). While TSI, SOD,

ACPD
12, 23913–23974, 2012

ENSO, and perhaps AMO are important for understanding past climate (e.g. Sect. 4 of Canty et al., 2012), none of these parameters are central to the predictability of climate on half-century time scales. We use TSI, SOD, ENSO, AMO, PDO, and IOD in the regression because this allows us to infer optimal estimates for γ as a function of prescribed NAA RF and OHE. The PDO and IOD terms are extremely minor (Figs. 6 and 7 of Canty et al., 2012) and although included are not shown. A description of the treatment of TSI, SOD, ENSO, AMO, PDO, and IOD is given in Sect. 2.2.5.

Simulations referred to below as "Best Fit" are based on values of the regression coefficients ($C_{j,j=0\text{ to }6}$) and the sensitivity parameter (γ) found such that the Cost Function is minimized, for specified GHG RF_i, NAA RF_i and OHE, over the time period of observation of $\Delta T_{OBS\ i}$ (start of 1900 to end of 2010). Values of γ, Ω, and the regression coefficients are then used to estimate ΔT for the future, using values of GHG RF_i and NAA RF_i from one of the RCP scenarios.

Simulations referred to below as "Acceptable Fit" are based on values of the regression coefficients and the sensitivity parameter found such that reduced chi-squared, defined as:

$$\chi^2 = \frac{1}{(N_{\text{MONTHS}} - N_{\text{FITTING PARAMETERS}} - 1)} \sum_{i=1}^{N_{\text{MONTHS}}} \frac{1}{\sigma^2_{\text{OBS}\ i}} (\Delta T_{\text{OBS}\ i} - \Delta T_{\text{MDL}\ i})^2 \quad (8)$$

where $N_{\text{FITTING PARAMETERS}}$ equals 8 (e.g. Canty et al., 2012), is less than 2. Technically, a value of $\chi^2 \leq 2$ indicates that a model agrees with observations, to within the 2-sigma uncertainty of measurement. Determination of the range of model parameters for which $\chi^2 \leq 2$ involves first specifying NAA RF_i and OHE, then varying γ in step-wise fashion. Regression coefficients and the associated value of χ^2 are then found for each value of γ. As shown in Sect. 3.3, use of $\chi^2 \leq 2$ to define the range of acceptable fits to the climate record is important for diagnosing the behavior of GCMs.

ACPD
12, 23913–23974, 2012

2.2 Data description

The data used in our analysis are described below. Sections 2.2.1 to 2.2.4 provide a detailed description of the most important parameters for this paper. A brief description of other parameters is provided in Sect. 2.2.5. A more detailed description of all parameters, including web addresses from which data files were obtained, is given by Canty et al. (2012).

2.2.1 Temperature

The regression analysis is based on modeling the variations of global, monthly mean surface temperature anomalies ($\Delta T_{\mathrm{OBS}\ i}$ in Eq. 1). Here we focus entirely on HadCRUT4, the latest data set provided by the Hadley Centre of the United Kingdom Met Office and the Climate Research Unit of University of East Anglia (Morice et al., 2012). We use the short hand abbreviation CRU4, throughout, to refer to this data set. At time of paper submission, the CRU4 record for ΔT was available from January 1900 to December 2010. This global record of surface temperature combines the HadSST3 record of sea surface temperature (SST) (Kennedy et al., 2011a,b), which has been adjusted to account for the sampling bias described by Thompson et al. (2008), with the CRUTEM4 record of land temperature (Jones et al., 2012).

2.2.2 Radiative forcing due to GHGs

The radiative forcing due to greenhouse gases (GHG RF_i in Eq. 1) is based on global, annual mean mixing ratios of CO_2, CH_4, and N_2O provided by the RCP database prepared for the upcoming IPCC report (Meinshausen et al., 2011; van Vuuren et al., 2011a). We interpolate annual abundances to a monthly time grid. Monthly values of radiative forcing due to CO_2, CH_4, and N_2O, relative to year 1750, are found using formula in Table 6.2 of IPCC (2001). The radiative forcing due to tropospheric O_3 (hereafter, O_3) is obtained from files posted at the Potsdam Institute for Climate Impact

ACPD
12, 23913–23974, 2012

Research, RCP webpage (Meinshausen et al., 2011) (hereafter, RCP Potsdam). Radiative forcing due to halogens involves a combination of projected abundances from RCP, WMO (2011), and Velders et al. (2009), as described below and in the Supplement.

Figure 1 shows time series of GHG RF due to CO_2, CH_4, O_3, halocarbons, and N_2O for the four RCP scenarios. Section 3.2 is based exclusively on the RCP 8.5 scenario (Riahi et al., 2007, 2011). The 8.5 label refers to a total RF of climate, due to GHGs and aerosols, of 8.5 W m^{-2} in year 2100. Our focus is examination of the evolution of ΔT at the time CO_2 reaches 2 × pre-industrial levels, which is projected to occur in year 2053 in the RCP 8.5 scenario. Consequently, our simulations extend to year 2060. The RF due to GHGs rises to about 6.5 W m^{-2} in year 2060 according to RCP 8.5, about twice the present day RF of climate due to GHGs (Fig. 1a). The bulk of the increase is due to rising CO_2.

Section 3.3 shows projections of ΔT for all four of the RCP scenarios. The RF due to GHGs for year 2060 in the RCP 6.0 scenario (Masui et al., 2011) is about the same as for the RCP 4.5 scenario (Thomson et al., 2011) (Fig. 1b, c). After year 2060, emissions of GHGs continue to steadily rise in the RCP 6.0 scenario whereas emissions sharply decline in the RCP 4.5 scenario (e.g. Fig. 4 of Meinshausen et al., 2011). The RCP 3−PD scenario (van Vuuren et al., 2011b) has total RF of climate peaking at 3.0 W m^{-2} around 2040, then declining to a value of 2.6 W m^{-2} by the end of this century (consequently this scenario is sometimes called RCP 2.6). The nomenclature PD refers to "peak and decline". The initial decline of GHG RF in RCP 3−PD is apparent in Fig. 1d. The peak value of 3.0 W m^{-2} refers to the sum of anthropogenic GHG RF (warming) and anthropogenic aerosol RF (cooling). As described in Sect. 2.2.3, NAA RF for RCP 3−PD is about −0.5 W m^{-2} for our baseline simulation, leading to a peak total human RF of ∼3.0 W m^{-2} occurring around year 2040.

Our treatment of the RF of halocarbons is a bit different from RCP. Future mixing ratios of CFC-11, CFC-12, CFC-113, CCl_4, HCFC-141b, Halon 1301, and Halon 2402 are taken from WMO (2011), rather than RCP, because WMO (2011) provides a more

ACPD
12, 23913–23974, 2012

recent projection that agrees closely with atmospheric observations of these species (Chap. 1 and 5 of WMO, 2011). Additionally, projections of HFC-125, which has a GWP of 3500 for a 100 yr time horizon (Table 2.14 of IPCC, 2007), are much lower in the RCP scenarios compared to Velders et al. (2009). As described in Supplement, we have formed High, Middle, and Low scenarios for the direct RF from halocarbons. Our halocarbon scenarios vary because it is uncertain whether future mixing ratios of HFC-125 will be large as projected by Velders et al. (2009) or as low as projected by RCP. We use our High halocarbon scenario for runs using RCP 8.5, the Middle scenario for RCP 6.0 and 4.5, and the Low scenario for RCP 3−PD.

2.2.3 Radiative forcing due to aerosols

Figures 2, 3, and 4 detail our treatment of net anthropogenic aerosol radiative forcing (NAA RF_i in Eq. 2). The estimate of NAA RF is based on values of direct RF of aerosols that presently cool (sulfate, mineral dust, ammonium nitrate, fossil fuel organic carbon) and direct RF of aerosols that presently heat (fossil fuel black carbon, biomass burning organic and black carbon) from RCP Potsdam. We use our own estimate for direct RF by sulfate aerosols ($RF_{SULFATE\text{-}DIR}$) for years up to and including 2005, formed by combining sulfur emissions from Smith et al. (2011) with RF estimates of Stern (2006a), as described in Sect. 3.2.2 of Canty et al. (2012). For 2006 and onwards, $RF_{SULFATE\text{-}DIR}$ is based on information provided by RCP Potsdam. We made this choice because historical values of $RF_{SULFATE\text{-}DIR}$ from RCP Potsdam show a temporal variation that does not match the time evolution of emissions from either Smith et al. (2011) or Stern (2006b). This detail is more important for our companion paper focused on past climate (Canty et al., 2012) than this paper. For consistency we use the same model structure for NAA RF as our companion paper.

The total RF due to aerosols is much larger than direct aerosol RF, due to many feedbacks (e.g. Sect. 2.4.1 of IPCC, 2007). The value of NAA RF is highly uncertain (e.g. Schwartz et al., 2007) and has proven difficult to narrowly constrain from empirical studies of aerosols and clouds (e.g. Morgan et al., 2006; Table 2.12 of IPCC, 2007). Canty

ACPD
12, 23913–23974, 2012

et al. (2012) described the use of scaling parameters, α_{COOL} and α_{HEAT}, designed to address the uncertainty in NAA RF as well as the fact that total RF exceeds direct RF by large amounts (e.g. Table 2.12 of IPCC, 2007; Storelvmo et al., 2009). Throughout this paper, year 2005 is used as a benchmark for net anthropogenic aerosol radiative forcing due to the large number of tables and figures in IPCC (2007) that quantify RF of anthropogenic aerosols between 1750 (when NAA RF was essentially zero) and 2005.

Figure 2a shows time series of total RF due to various anthropogenic aerosols that cool, found using $\alpha_{COOL} = 2.4$, applied to direct RF terms for RCP 8.5. This value of α_{COOL} is the ratio of $-0.96\,W\,m^{-2}$ (our best estimate of total RF due to sulfate in 2005; Sect. 3.2.2 of Canty et al., 2012) to $-0.40\,W\,m^{-2}$ (the value of $RF_{SULFATE\text{-}DIR}$ in 2005; Table 2.12 of IPCC, 2007). We have scaled the RCP Potsdam values of direct RF due to mineral dust, ammonium nitrate, and organic carbon by the same value of $\alpha_{COOL} = 2.4$, to obtain the curves shown in Fig. 2a.

Figure 2b is analogous to Fig. 2a, except for aerosols that heat. Here, $\alpha_{HEAT} = 2.4$ is used. This value for α_{HEAT} is needed to match the IPCC (2007) best estimate for NAA RF in year 2005 (hereafter, NAA RF_{2005}) of $-1.0\,W\,m^{-2}$ (Appendix D, Canty et al., 2012). Figure 2c shows a time series of NAA RF, with NAA RF_{2005} marked. It is coincidental that both α_{COOL} and α_{HEAT} have values of 2.4 for our baseline simulation.

Figure 3 shows time series of NAA RF for the four RCP scenarios, for values of α_{COOL} and α_{HEAT} tied to various estimates of NAA RF_{2005}. Figure 3a corresponds to scaling parameters that force NAA RF_{2005} to equal $-0.40\,W\,m^{-2}$, the upper limit (least cooling) of this quantity according to our analysis of Table 2.12 of IPCC, 2007 (Appendix D, Canty et al., 2012). Figure 3b shows NAA RF for values of the scaling parameters used in Fig. 2. The black line (pre-2005) combined with the red line (post-2005) in Fig. 3b is the same as the black line in Fig. 2c. Figure 3b shows the baseline time series of NAA RF used in Sect. 3.2. Finally, Fig. 3c shows NAA RF for scaling parameters that force NAA RF_{2005} to equal $-2.2\,W\,m^{-2}$, the lower limit (most cooling) of this quantity according to Table 2.12 of IPCC, 2007.

ACPD
12, 23913–23974, 2012

A major hurdle facing modern studies of climate change is that none of the NAA RF time series shown in Fig. 3 can be ruled out based on assessments of the literature such as Morgan et al. (2006) or Chapter 2 of IPCC (2007). Studies published since IPCC (2007) have provided some constraint: for instance, the analysis of atmospheric energy balance measurements and ocean heat transport by Murphy et al. (2009) suggests NAA RF around year 2000 was about $-1.7\,W\,m^{-2}$ and excludes values of NAA RF with cooling tendency less than $-1.0\,W\,m^{-2}$. Hansen et al. (2011) suggest various climate records can be best fit if contemporary NAA RF is $-1.6 \pm 0.3\,W\,m^{-2}$. Conversely, the largest aerosol cooling within the 9 GCMs analyzed by Kiehl (2007) for the contemporary atmosphere is $-1.4\,W\,m^{-2}$ and the greatest aerosols cooling of the various GCM ensemble calculations of Stott and Forest (2007) is $-1.1\,W\,m^{-2}$. These numbers suggest GCMs may not be sampling the full range of uncertainty of NAA RF, an issue emphasized by Schwartz et al. (2007).

To complicate matters further, there are infinitely many combinations of α_{COOL} and α_{HEAT} that yield the same value of NAA RF_{2005}. The red line on Fig. 4 represents the isopleth of NAA $RF_{2005} = -1.0\,W\,m^{-2}$, as a function of α_{COOL} and α_{HEAT}. Black lines represent isopleths for different values of NAA RF_{2005}. The green dashed lines represent the uncertainty range of NAA RF_{2005} we have computed, $-0.4\,W\,m^{-2}$ to $-2.2\,W\,m^{-2}$, from Table 2.12 of IPCC (2007) (Appendix D of Canty et al., 2012). The blue dashed lines represent the uncertainty range of NAA RF_{2005} in 9 GCMs analyzed by Kiehl (2007).

The lines marked "High Road", "Middle Road", and "Low Road" in Fig. 4 show three possible ways α_{COOL} and α_{HEAT} can be combined to arrive at the same value of NAA RF_{2005}. As shown below, simulations of climate found using our MLR model are nearly identical regardless of which road is chosen. This provides a tremendous simplification to our treatment of the uncertainty in NAA RF: all that matters is the value of NAA RF for a time near present, rather than the particular values of scaling parameters used to arrive at this value (at least for the range of values for α_{COOL} and α_{HEAT} bounded by the "High Road", "Low Road", and "Empirical Range" on Fig. 4). This insensitivity to how the

ACPD
12, 23913–23974, 2012

scaling parameters are combined is due ultimately to the following aspects of aerosol radiative forcing: (1) all precursor emissions have generally risen over time driven by population growth and economic productivity; (2) cooling is dominated by sulfate and heating is dominated by black carbon; (3) the recent decline in sulfate emission due to technological advance generally tracks the recent decline in black carbon emission (Myhre et al., 2001; Stern, 2006b; Smith et al., 2011). Thus, while use of two scaling parameters is a simple approach, these parameters provide an important avenue for exploration of the uncertainty in NAA RF that is both directly tied to precursor emissions and also captures a wide range of physical possibilities.

2.2.4 Ocean heat export

The radiative forcing perturbation due to rising levels of GHGs can either cause a rise in the temperature of the atmosphere and ocean skin or it can cause a rise in the temperature of the water column of the world's oceans (e.g. Hansen et al., 2011). The oceanographic community has estimated the rise in ocean heat content (OHC) based on measurements of water temperature by a variety of sensor systems and data assimilation techniques (e.g. Carton and Santorelli, 2008). Generally the focus has been on defining the rise of OHC for the upper 700 m of the ocean, which according to GCM calculations lags an atmospheric perturbation by about 6 yr (Schwartz, 2012). Hereafter, OHC will refer exclusively to the heat content of the upper 700 m of the world's oceans.

Church et al. (2011) provide an estimate of OHC from 1950 to 2009. Their estimate, an update to data described in Domingues et al. (2008), is based on analysis of data provided by expendable bathy-thermograph (XBT) devices, more accurate conductivity temperature depth (CTD) probes (available since the 1980s), and an array of ~3000 drifting floats (from 2001 onwards). Church et al. (2011) apply a time-dependent, depth independent, fall rate correction to their XBT data.

Ocean Heat Export (OHE), the numerator of Eq. (5), represents the flow of energy from the atmosphere into the oceanic water column. OHE (heat flux) is the derivative

ACPD
12, 23913–23974, 2012

with respect to time of OHC (energy) divided by the surface area of the ocean. One approach for using measurements of OHC could be to constrain a model to match dOHC/dt at each time step (data are provided on an annual basis, but we could interpolate the rate of change of OHC to monthly time steps). There are numerous reasons why we do not take this approach, the most important being our desire to use an approach that is physically consistent with the OHC data but also allows us to start our model in 1900 (before OHC is available) and extend the model into the future. We therefore compute a single number from the OHC measurement, the mean value of OHE over the time of measurement, and deduce for each model run the fraction of anthropogenic radiative forcing (GHG RF + NAA RF) that must flow into the ocean to match OHE over the period of observation. This fraction, represented by Ω in Eq. (5), is then applied at each model time step (Eq. 4).

A linear, least squares fit to the OHC measurements of Church et al. (2011) indicates that OHC rose by 21.3×10^{22} J from start of 1950 to end of 2009. Dividing this value by the surface area of the ocean and the time interval of the data yields a value for OHE = $0.347\,\mathrm{W\,m^{-2}}$ for the numerator of Eq. (6). Typical model runs using OHE from Church et al. (2011) yield values of $\Omega \approx 0.20$ (value of Ω varies slightly based on specification of NAA RF_{2005}).

Gouretski and Reseghetti (2010) provide a starkly different estimate of OHC than Church et al. (2011). Gouretski and Reseghetti (2010) have established a new fall rate correction for XBT data, based on side-by-side comparisons of XBT and CTD data. Gouretski and Reseghetti (2010) suggest OHC rose by 19.2×10^{22} J from 1990 to 2005, which leads to OHE = $1.22\,\mathrm{W\,m^{-2}}$ for Eq. (6). As shown below, a comparison of OHC time series from Church et al. (2011) and Gouretski and Reseghetti (2010) reveals differences much larger than the uncertainty estimate of the Church et al. (2011) data (we have been unable to find uncertainties for the Gouretski and Reseghetti OHC estimate). Typical model runs using OHE from Gouretski and Reseghetti (2010) yield values of $\Omega \approx 0.37$.

ACPD
12, 23913–23974, 2012

Initial calculations are based on the Church et al. (2011) measurement of OHC. The sensitivity of model results to OHC is explored by using data from Gouretski and Reseghetti (2010), as well as calculations for OHC from Church et al. (2011) cut in half (hereafter 0.5×Church) and OHC from Gouretski and Reseghetti (2010) doubled (hereafter 2.0×Gouretski), which provide extreme lower and upper limits to OHC of the upper ocean, respectively.

2.2.5 Other parameters used in the regression

The regression model (Eq. 2) also considers proxies for the effect on ΔT of volcanoes strong enough to perturb stratospheric optical depth (SOD), the 11-yr solar cycle in total solar irradiance (TSI), the El Niño-Southern Oscillation (ENSO), and variations in the strength of the Atlantic Meridional Overturning Circulation (AMOC) as reflected by the Atlantic Multidecadal Oscillation (AMO), all shown in ladder plots to follow. Proxies for the Pacific Decadal Oscillation (PDO) and the Indian Ocean Dipole (IOD) are included for completeness. As described by Canty et al. (2012), there is no significant contribution to ΔT from the PDO and the IOD.

The value of SOD used in the regression is from Sato et al. (1993), which is maintained on a Goddard Institute for Space Studies server (URLs of many proxies are given in Appendix B of Canty et al., 2012). The TSI record is based on the Naval Research Laboratory reconstruction of Lean (2000) and Wang et al. (2005), updated by J. Lean (private communication, 2012). We use the multivariate ENSO index of Wolter and Timlin (2011), provided on a National Oceanic and Atmospheric Administration (NOAA) server. The PDO index is based on an empirical orthogonal function analysis of Zhang et al. (1997), provided on a University of Washington website. The IOD is modeled using an index provided by the Japan Agency for Marine-Earth Science and Technology (Saji et al., 1999).

The AMO index is a measure of the variability of SST in the North Atlantic Ocean (Schlesinger and Ramankutty, 1994). As detailed in Sect. 3.2.3 of Canty et al. (2012), we have obtained SST records from two data centers, the Hadley Centre (HadSST3)

ACPD
12, 23913–23974, 2012

(Kennedy et al., 2011a,b) and NOAA (Kaplan Extended SST V2) (Enfield et al., 2001) and formed our own AMO indices, because the regression coefficient for AMO (variable C_4 in Eq. 2) is sensitive to how the AMO index is detrended. An AMO index detrended using a linear fit (Enfield et al., 2001) results in a considerably larger regression coefficient than an AMO index detrended using global SST (Trenberth and Shea, 2006). AMO indices formed using SST from HadSST3 provide nearly identical results to AMO indices formed using SST from Kaplan Extended SST V2.

Here we exclusively use an AMO index detrended using global SST, based on the HadSST3 data record. In the notation of Canty et al. (2012), we use the $AMO_{Had3\ SST}$ index. As described in our companion paper, better fits to the CRU4 climate record are obtained using AMO indices detrended either using linear fit or the non-linear, time varying anthropogenic radiative forcing of climate. There is scientific debate regarding whether variations in the AMO are a response to ocean salinity and sea ice or a response to tropospheric aerosols and volcanic aerosols that reach the stratosphere (Sect. 4.3 of Canty et al., 2012). The $AMO_{Had3\ SST}$ index is the most benign choice we could make. Choice of AMO, provided the index is detrended, has no effect on the conclusions of this study (see Supplement).

Following Lean and Rind (2009), we have propagated variations of TSI into the future by repeating the last two solar cycles. As shown in the ladder plots that follow, future variations in TSI have a very small ripple effect on future ΔT. Lean and Rind (2009) also included a notional future major volcanic eruption as well as a future major ENSO event. We have decided to "flat line" indices for SOD, ENSO, AMO, PDO, and IOD into the future. If consensus emerges that variations in the strength of the AMOC exert a major influence on global climate and the AMO can be used as a proxy for this influence, as suggested by Knight et al. (2005), Stouffer et al. (2006), Zhang et al. (2007), and Medhaug and Furevik (2011), then future projections of ΔT using models such as this should explore projecting the AMO index into the future. We have decided to zero out the future AMO index, because the AMO is not central to our study of the interplay between γ, NAA RF, and OHE on half-century timescales. Since we use

ACPD
12, 23913–23974, 2012

a detrended AMO index, we do not consider the possibility that the strength of the AMOC has decreased monotonically over time due to rising GHGs, a suggestion not yet borne out by observation (Box 5.1 of IPCC, 2007; Willis, 2010).

3 Results

3.1 Overview of calculations

Here we describe use of the empirical model of global climate to project ΔT to year 2060. Our work builds on Lean and Rind (2009). However, Lean and Rind (2009) projected climate for a single value of NAA RF, using the best fit to their model Cost Function. They did not explicitly treat ocean heat export, but they did include a time lag between GHG forcing and atmospheric response that could arguably be termed a surrogate for explicit treatment of OHE. Our effort differs from Lean and Rind (2009) in three ways: (1) we quantify the impact of uncertainty in NAA RF on our regressions; (2) we model OHE and show results for disparate estimates of OHC; and, (3) we explore model parameter space in terms of χ^2, which quantifies how well the climate record can be simulated.

Section 3.2 provides an overview of the interplay of radiative forcing due to aerosols, climate feedback, and ocean heat export within the context of our model. The RCP 8.5 scenario for GHG emissions (Riahi et al., 2007, 2011) is primarily used. Section 3.3 shows projections of future global mean surface temperature, out to year 2060, for the four RCP scenarios (8.5, 6.0, 4.5, and 3−PD). We conduct simulations to year 2060 because understanding how global temperature will rise when CO_2 is projected to double (year 2053 in the RCP 8.5 scenario) is the major focus of our study. Our forecast temperature covers a similar time period as that examined by the ensemble GCM calculations of Rowlands et al. (2012). Section 3.4 provides a critical evaluation of the use of equilibrium climate sensitivity to diagnose GCM behavior.

ACPD
12, 23913–23974, 2012

3.2 Aerosols, climate feedback, and ocean heat

Figure 5 shows "ladder plots" of the monthly, global mean surface temperature anomaly (ΔT) reported by CRU4, from 1900 to the end of 2010, with modeled ΔT for two regressions based on GHG abundance and aerosol forcing from RCP 8.5. Results are shown for "best fit" regressions: i.e. the Cost Function has been minimized. Figure 5a shows a regression where NAA RF_{2005} was set to $-0.4\,W\,m^{-2}$ (Model 1), the upper limit (least cooling) according to our analysis (Appendix D, Canty et al., 2012) of Table 2.12 of IPCC (2007). Figure 5b shows results for NAA $RF_{2005} = -2.2\,W\,m^{-2}$ (Model 2), the lower limit (most cooling). Time series of NAA RF used for Models 1 and 2 are shown in Fig. 3a, c, respectively.

The rungs of the Fig. 5 ladder plots show computed contributions to ΔT from volcanoes (using SOD as a proxy), the solar cycle (using TSI), humans (combination of GHG and aerosols), El Niño, and variations in the strength of the Atlantic Meridional Overturning Circulation (AMOC) (using AMO as a proxy). The AMO has been detrended using global SST, which leads to the smallest influence of the AMOC on the regression (Sect. 4.1 of Canty et al., 2012). The second to last rung of each ladder plot shows RF due to anthropogenic GHGs and aerosols and the final rung compares modeled and measured OHC.

Simulations in Fig. 5 have been constrained to match the OHC measurements of Church et al. (2011). The model formulation for OHE, based on the export to the ocean of a constant fraction of the total anthropogenic RF (parameter Ω), provides a good simulation of observed OHC (bottom rungs, Fig. 5).

The value of χ^2 from each "best fit" regression is recorded on the top rung of each ladder plot. The value of ΔT in 2053 (ΔT_{2053}), the year CO_2 doubles according to RCP 8.5, is highlighted by placing on each plot ΔT_{2053} from the other regression. There is a 0.57 °C difference in ΔT_{2053} from these two projections, both of which provide nearly identical simulations of the CRU4 temperature record. Indeed, one would be hard pressed, based on the comparison of measured and modeled ΔT in the top rungs

ACPD
12, 23913–23974, 2012

of Fig. 5, to distinguish between the two simulations. As has been well established (e.g. Kiehl, 2007; Murphy et al., 2009; Hansen et al., 2011), external constraint on either γ or NAA RF for a time close to present is needed to break this dichotomy.

The Anthropogenic Forcing rungs of the ladder plots illustrate the cantilevering between climate feedback (sensitivity parameter γ) and NAA RF that results in this dichotomy. When NAA RF is set to the extreme upper limit of least cooling (Model 1), the temperature record can only be fit if climate feedback is small ($\gamma = 0.16$; little amplification of GHG RF). The curve labeled GHG on this rung shows $(1 + \gamma)$(GHG RF). As a result, net anthropogenic RF of climate (GHG RF + NAA RF; curve labeled Net) is close to the direct GHG RF because both γ and NAA RF are small.

The anthropogenic RF of climate is quite different for Model 2. When aerosol cooling is large, the CRU4 data can only be fit assuming considerable amplification of GHG RF ($\gamma = 0.73$). Between ~1950 and present, net anthropogenic RF of climate reflects the difference of two large terms: GHG RF amplified by large γ and considerable cooling due to aerosols. However, all of the RCP scenarios project that NAA RF will level off and slowly decline by the time CO_2 doubles (Fig. 3). For Model 2, GHG RF will grow quickly once NAA RF declines, because whatever feedbacks are needed to explain past climate are assumed to continue into the future. By 2060, the net anthropogenic RF for Model 2 is much larger than net anthropogenic RF for Model 1, even though both models are based on the same RCP 8.5 GHG abundance and emission scenario.

Figure 5 and the other ladder plots demonstrate, as is well known, that the ~110 yr rise in ΔT is due to the increase in GHG RF of climate over this period of time. Despite the complexity in predicting future climate, the near monotonic rise of ΔT from 1900 to 2010 is clearly associated with anthropogenic radiative forcing of climate (second to last rung) that provides the basis for the only term of the regression (Human rung) that rises over time in a manner comparable to the magnitude of observed ΔT.

We now turn our attention to ocean heat export. Figure 6 shows simulations of ΔT for two regressions that use NAA $RF_{2005} = -1.0\ W\ m^{-2}$, the IPCC (2007) best estimate of this parameter (Appendix D of Canty et al., 2012). RCP 8.5 is used for both simulations

ACPD
12, 23913–23974, 2012

shown in Fig. 6. Model 3 (Fig. 6a) shows results constrained to the OHC measurement of Church et al. (2011) whereas Model 4 (Fig. 6b) is constrained to match OHC of Gouretski and Reseghetti (2010). The bottom rung of each ladder plot shows that a much steeper rise in OHC over time is needed to match the data of Gouretski and Reseghetti (2010).

Modeled ΔT in year 2053, when CO_2 doubles, is essentially independent on OHC. A value of $\gamma = 0.35$ is needed to balance the OHC data of Church et al. (2011) and minimize the cost function, resulting in $\Omega = 0.20$. In other words, for Model 3, 20 % of the anthropogenic RF perturbation is exported to the ocean. Model 4, constrained to match the Gouretski and Reseghetti (2010) observation of OHC, produces $\gamma = 0.59$ and $\Omega = 0.37$ for the best fit to the CRU4 data. In order to match the observed temperature record, the export of more heat to the ocean (larger value of Ω) is offset by greater climate feedback (larger value of γ). Projected ΔT_{2053} differs by only 0.06 °C for these two best fit simulations (ΔT_{2053} is 1.45 °C for Model 3 and 1.39 °C for Model 4).

At face value one might think that the MLR simulations shown in Fig. 6 are contradictory to the notion, as expressed for instance by Knutti et al. (2002), that climate sensitivity is strongly dependent on ocean heat uptake. However, the two simulations shown in Fig. 6 are associated with quite different values of γ.

Climate sensitivity, denoted $\Delta T_{2\times CO_2}$, is defined as "the global annual mean surface air temperature change experienced by the climate system after it has attained a new equilibrium in response to a doubling of atmospheric CO_2" (Sect. 8.6.2.1 of IPCC, 2007). In our notation, $\Delta T_{2\times CO_2}$ is expressed as:

$$\Delta T_{2\times CO_2} = \lambda(1+\gamma)5.35 \ln\left(\frac{CO_2^{FINAL}}{CO_2^{INITIAL}}\right) \quad (9)$$

where $CO_2^{FINAL} = 2 \times CO_2^{INITIAL}$ and the logarithmic dependence of the CO_2 RF is the IPCC (2007) expression originally published by Myhre et al. (1998).

Evaluating Eq. (9) for Models 3 and 4 yields climate sensitivities of 1.50 °C and 1.77 °C, respectively. As the fraction of heat exported to the ocean rises (i.e. Model

ACPD
12, 23913–23974, 2012

4), the temperature found at the time CO_2 doubles (year 2053) lies further from equilibrium. Of course, ΔT_{2053} and $\Delta T_{2\times CO_2}$ also differ because ΔT_{2053} takes into consideration RF perturbation due to GHGs other than CO_2 and aerosols, whereas the notional equilibrium climate sensitivity $\Delta T_{2\times CO_2}$ considers only RF from CO_2. The difference between $\Delta T_{2\times CO_2}$ for Models 3 and 4, despite nearly identical projections of future ΔT, is a microcosm of the complication endemic in use of $\Delta T_{2\times CO_2}$ to evaluate GCMs.

Heretofore we have considered only "best fits" of the regression, found by minimizing the model Cost Function. The true power of our framework resides in the ability to explore the model parameter space in terms of the metric χ^2. Physically, a value of $\chi^2 \leq 2$ indicates that a model agrees with observations, within the 2-sigma measurement uncertainty. We are not suggesting such a literal interpretation because values of χ^2 are affected by the invariably subjective nature of specification of measurement uncertainty. For instance, our analysis of the Berkeley Earth Group land temperature record (Rohde et al., 2011) never achieves anywhere close to $\chi^2 = 2$, because of the vanishingly small uncertainties associated with this data record (Table 2 of Canty et al., 2012). Nonetheless, we use the $\chi^2 \leq 2$ below because simulations subject to this constraint follow the CRU4 record of ΔT in a manner visually similar to the behavior of the GCM ensemble (gold lines) shown in Fig. 9.5a of IPCC (2007).

Figure 7 shows values of χ^2 and ΔT_{2053} as a function of NAA RF_{2005} and γ. All simulations are driven by GHG and aerosol forcings from RCP 8.5 and are constrained to match the OHC record of Church et al. (2011). Figure 7a, b shows results where scaling parameters α_{COOL} and α_{HEAT} are taken, as a function of NAA RF_{2005}, along the "High Road" of Fig. 4; Fig. 7c, d uses parameters along the "Middle Road" and Fig. 7e, f is based on the "Low Road". The left panels of Fig. 7 show χ^2 and include a white line denoting $\chi^2 = 2$. Any simulation that lies within this white boundary is deemed to be an "acceptable fit" of the climate record.

The right panels of Fig. 7 show ΔT_{2053} for the acceptable fit region of parameter space. We further restrict depiction of ΔT_{2053} by using color to denote model results for values of NAA RF_{2005} that lie within the empirical range assessed by IPCC (2007).

ACPD
12, 23913–23974, 2012

Appendix D of Canty et al. (2012) documents our determination of the empirical range to be $-2.2\,W\,m^{-2}$ to $-0.4\,W\,m^{-2}$, based on Table 2.12 of IPCC (2007).

Panels b, d, and f of Fig. 7 include numerical values for the range of ΔT_{2053} encompassed by all acceptable fit regressions for which NAA RF_{2005} lies within the empirical range. For aerosol scaling parameters along the Middle Road (Fig. 7d), ΔT_{2053} is projected to lie between 0.8 °C and 2.22 °C. The range of ΔT_{2053} shown in Fig. 7b (High Road) and Fig. 7f (Low Road) are nearly identical to the range in Fig. 7d. This reinforces our notion that provided whatever interactions occur between aerosols, clouds, and surface albedo remain stable over time, climate projections are sensitive only to the value of NAA RF_{2005} or NAA RF for some other year close to present, rather than the specific combination of scaling parameters used to arrive at NAA RF_{2005}. Hereafter, all model results will use scaling parameters along the Middle Road.

Figure 8 is analogous to Fig. 7, except results are shown for a model constrained to match OHC from Gouretski and Reseghetti (2010). The range of ΔT_{2053} found using OHC from Gouretski and Reseghetti (2010) is 0.8 °C and 2.08 °C, nearly identical to the range found using OHC from Church (2011). The $\chi^2 = 2$ boundary on Fig. 8 is displaced vertically relative to Fig. 7, due to the need for higher values of γ (stronger climate feedback) to balance larger ocean heat export needed to match the OHC data of Gouretski and Reseghetti (2010). Consequently, larger values of $\Delta T_{2\times CO_2}$ (Eq. 9) are associated with model results shown in Fig. 8 compared to model results shown in Fig. 7, despite nearly identical ranges for ΔT_{2053} shown in Figs. 7d and 8b.

The dependence of the sensitivity parameter γ, ΔT_{2053}, and $\Delta T_{2\times CO_2}$ on both NAA RF_{2005} and OHC is summarized in Fig. 9. All simulations have been constrained by RCP 8.5. For illustrative purposes, we include simulations for which the OHC record of Gouretski and Reseghetti (2010) has been doubled (2×Gouretski) and the OHC record of Church et al. (2011) has been cut in half (0.5×Church), which represent extreme upper and lower limits for OHE. Model parameter Ω, the fraction of anthropogenic RF exported to the ocean, equals 0.11 for 0.5×Church and 0.54 for 2×Gouretski. Regressions were conducted for 5 values of NAA RF_{2005}, all based on scaling parameters

ACPD
12, 23913–23974, 2012

along the "Middle Road" of Fig. 4: the IPCC (2007) lower and upper empirical limits ($-2.2\,W\,m^{-2}$ and $-0.4\,W\,m^{-2}$), the IPCC (2007) best estimate ($-1.0\,W\,m^{-2}$), and the limits of NAA RF_{2005} within 9 GCMs analyzed by Kiehl (2007) ($-1.4\,W\,m^{-2}$ and $-0.6\,W\,m^{-2}$). Symbols are for best fits. The error bars in Fig. 9b reflect the range of ΔT_{2053} for acceptable fits, placed at the upper and lower limits of NAA RF_{2005}.

Figure 9 illustrates five points important for understanding the question posed by Kiehl (2007):

a. best fits to the past climate record can only be obtained for compact relations of the sensitivity parameter γ and NAA RF_{2005} (Fig. 9a);

b. the actual best fit γ versus NAA RF_{2005} relation is sensitive to OHE (Fig. 9a);

c. if aerosols presently exert little effect on global climate (leftmost half of NAA RF_{2005} empirical range) then temperature at the time CO_2 will double (ΔT_{2053}) depends nearly entirely on γ, whereas if aerosols presently exert a strong cooling influence ΔT_{2053} will depend mainly on γ and weakly on OHE (Fig. 9a, b);

d. the range of ΔT_{2053} introduced by considering all acceptable fits to the climate record for a single value of NAA RF_{2005} (length of error bars, ~0.85 °C) is comparable to the range in ΔT_{2053} due to uncertainty in NAA RF_{2005} and OHE for best fits (difference between leftmost red square and rightmost blue triangle, ~0.7 °C) (Fig. 9b);

e. the difference between $\Delta T_{2\times CO_2}$ and ΔT_{2053} depends on OHE: simulations with small OHE project future temperature when CO_2 doubles to be close to the equilibrium climate sensitivity, whereas simulations with large OHE project temperature when CO_2 doubles to be far from the equilibrium climate sensitivity (Fig. 9d).

These points will be revisited in Sect. 3.4, which addresses the complications of climate sensitivity, as well as Sect. 4, which relates our findings to the literature.

ACPD
12, 23913–23974, 2012

3.3 Future temperature

Here we document the behavior of future temperature anomalies projected to year 2060, for regressions that provide either best fits or acceptable fits to observed ΔT. Figures are designed to address the question posed by Kiehl (2007). Our regression model projects future ΔT in a manner that mimics the behavior of GCMs. Advantages of the regression model are that all calculations shown in this section can be carried out in an afternoon on a modern work station and we have ready access to, and control over, model parameters. Of course, GCMs represent many quantities of societal interest, such as precipitation, drought, sea ice extent, sea level, etc that are not represented by our model.

Figure 10 shows temperature in year 2053 for regressions that provide acceptable fits to the CRU4 global, monthly mean surface temperature record, as a function of the sensitivity parameter γ and NAA RF_{2005}. The panels show results of simulations constrained by GHG and NAA RF forcings from the four RCP scenarios, as noted. All simulations have been constrained to match the OHC record of Church et al. (2011). Year 2053 has been chosen because this is when atmospheric CO_2 is projected to double, according to RCP 8.5.

Figure 10 shows that a wide range of future increases in ΔT are possible, based on projections constrained to match observed surface temperature over the past century and observed ocean heat content over the past half-century. The range of possible future temperature is narrowed if the reductions in GHG emissions assumed in the RCP 6.0, 4.5, and 3−PD scenarios are enacted. The radiative forcings due to GHGs in the RCP 6.0 and RCP 4.5 scenarios are quite similar for year 2053, accounting for the small difference in the projected warming shown in Fig. 10b, c. Figure 10 would look nearly identical had we used the Gouretski and Resgehetti (2010) estimate of OHC because, as detailed in Sect. 3.2, projections of ΔT are insensitive to ocean heat export (even though equilibrium climate sensitivity is sensitive to OHE).

ACPD
12, 23913–23974, 2012

Figure 11 shows ΔT_{2053} found used RCP 8.5, with the addition of two key lines. Figure 11a shows the "Best Fit" line defined by the minimum Cost Function for each value of NAA RF_{2005}. If we consider only the Best Fits of the regression, ΔT_{2053} would be projected to lie between 1.25 and 1.85 °C for RCP 8.5. Figure 11b shows the "Acceptable Fit" line defined by the range of ΔT_{2053} for which $\chi^2 \leq 2$. Considering all acceptable fits, ΔT_{2053} is projected to lie between 0.80 and 2.22 °C for RCP 8.5.

Figure 12 shows projections of ΔT vs. time, for the four RCP scenarios, for only the Best Fit solutions. All simulations have been constrained to match OHC from Church et al. (2011), but this figure would hardly differ had we used Gouretski and Reseghetti (2010). NAA RF_{2005} has been restricted to lie between $-1.4\,W\,m^{-2}$ and $-0.6\,W\,m^{-2}$ (denoted "Model Range"), the range used by the 9 GCMs examined by Kiehl (2007). The spread of projected ΔT is unrealistically small: Fig. 12 looks nothing like GCM projections of ΔT shown in Fig. 10.5 of IPCC (2007) and Fig. 1 of Rowlands et al. (2012). Best Fit projections from a MLR model provide little or no insight into the behavior of GCMs and are scientifically questionable because they lack consideration of uncertainties.

Figure 13 shows projections of ΔT from the set of acceptable fit simulations, sampled at each time step as exemplified by the "Acceptable Fit" line shown in Fig. 11b. Otherwise, the calculations shown in Fig. 13 are subject to the same constraints as Fig. 12. The spread in future ΔT is now considerable. Future ΔT can be seen to be dependent on net anthropogenic aerosol RF for the present day atmosphere, represented in our model by NAA RF_{2005}, as described in Sect. 3.2 and illustrated in Fig. 5. Even though we have placed a color bar on Fig. 13 denoting NAA RF_{2005}, there is not a one to one relationship between NAA RF_{2005} and future ΔT (except for the extrema). The values of NAA RF_{2005} used for the color bar reflect one particular realization of ΔT versus NAA RF_{2005} within the set of acceptable fits. This particular relation is the one along the "Acceptable Fit" line such as shown in Fig. 11b. We have placed a color bar on the plot because, in general, higher future temperature is related to stronger present day aerosol cooling. Future temperature would still be uncertain, even if present day NAA

ACPD
12, 23913–23974, 2012

RF could be precisely determined, because for each NAA RF_{2005} there are a multitude of values of γ that yield acceptable fits to the climate record.

Figure 14 is identical to Fig. 13, except we have used the IPCC (2007) empirical range of NAA RF_{2005}, $-2.2\,W\,m^{-2}$ to $-0.4\,W\,m^{-2}$. The spread in projected ΔT four decades into the future is large, driven by the ability of the model to simulate the past climate record nearly equally well for a wide range of values of the sensitivity parameter γ and NAA RF_{2005}. As explained in Sect. 3.2, if the net effect of aerosols is a small cooling (red colors, Fig. 14), climate feedback is small and temperature rise will be modest as NAA RF declines in the future. If the net effect of globally averaged anthropogenic aerosols is strong cooling for the present day atmosphere (blue colors, Fig. 14), the climate record can only be simulated assuming that a strong feedback (i.e. water vapor, clouds, and/or surface albedo) to the GHG RF perturbation has offset aerosol cooling. In this case, the strong feedbacks will likely persist as NAA RF declines in the future, leading to the upper end of the predicted range of ΔT for all panels of Fig. 14.

The cantilevering between NAA RF for the contemporary atmosphere and climate feedback, and the effect on future temperature, is well known (e.g. Kiehl, 2007; Schwartz et al., 2007; Hansen et al., 2011; Schwartz, 2012). Here, we have used the past climate record to map this relation onto RCP GHG abundance and aerosol precursor emission scenarios.

Figures 9 and 14 offer a possible explanation for why GCMs with quite different climate sensitivities are able to "simulate the global temperature record with a reasonable degree of accuracy" (Kiehl, 2007). Figure 14a includes the range of projected ΔT found by 21 GCMs, at the time CO_2 doubles, found for SRES A1B (Fig. 10.5 of IPCC, 2007). The ensemble average (horizontal line), the range of ΔT from all GCM values excluding a single outlier (thick vertical line), and representation of the outlier (thin vertical line) are shown. The similarity of the range of ΔT_{2053} for RCP 8.5 found by our MLR model subject to the constraint $\chi^2 \leq 2$ and the range reported by IPCC (2007) suggests, as postulated by Kiehl (2007), that much of the variability in projected ΔT from GCMs is due to differences in their treatment of climate feedback and NAA RF.

ACPD
12, 23913–23974, 2012

Schwartz et al. (2007) noted that if GCMs were to consider the full range of uncertainty in NAA RF for the present day atmosphere without any other constraints, then GCM calculations of the historical temperature record could not possibly agree with observed ΔT as well as indicated by Fig. 9.5 of IPCC (2007). Clearly some comparison of modeled and measured past temperature is done by the GCM community. Projections of future ΔT by a GCM that failed to provide a reasonable approximation to the known, historical climate record would not be taken seriously. Had the modeling community precisely "tuned" GCM simulations to provide nearly exact simulations of the climate record, there could perhaps be little divergence of projected future temperature, as in Fig. 12. However, if as we think is likely, GCM modeling groups compare to the observed temperature record and reject submission to the data archive simulations that are demonstrably wrong, then the resulting spread in projected ΔT could look like our Fig. 14.

One important limitation of our approach, the primary reason our projections of ΔT should be taken with some caution, is that we have assumed whatever climate feedback (sensitivity parameter γ) has occurred in the past will continue into the future. Since the 110 yr record of ΔT can be "best fit" extremely well based on this assumption (i.e. Figs. 5 and 6), this assumption can not be immediately invalidated. However, the overlap between projections of ΔT when CO_2 doubles from IPCC (2007) and our model estimate shown in Fig. 14a occurs for values of NAA RF_{2005} with large contemporary aerosol cooling: i.e. for NAA $RF_{2005} < -1.2\,W\,m^{-2}$. Inspection of GCMs reveals NAA RF_{2005} tends to be between $-0.6\,W\,m^{-2}$ and $-1.4\,W\,m^{-2}$ (Kiehl, 2007; Stott and Forest, 2007; Hansen et al., 2011). For this model range of NAA RF_{2005}, our projection of ΔT_{2053} lies below the ensemble IPCC (2007) GCM estimate. This tendency could be indicative of γ rising over time within GCMs, due to decreases in surface albedo driven by rapid, recent decline in seasonal sea ice, or other non-linear behavior of clouds or water vapor in response to anthropogenic RF. Had we allowed γ to vary over time, the model simulation shown by the red color in Fig. 14a would shift towards higher

ACPD
12, 23913–23974, 2012

values of ΔT_{2053}, because this model over estimates ΔT in the early 1900s and under estimates ΔT at the end of the record.

Rowlands et al. (2012) recently published projections of ΔT to year 2080 from a 9745 ensemble member GCM simulation (1656 controls and 8089 transients). Their ensemble involved perturbations to atmospheric physics, ocean circulation, and the sulfur cycle. These perturbations are analogous in a broad sense to our consideration of γ (surrogate for atmospheric physics), OHE, and NAA RF_{2005}. Rowlands et al. (2012) filtered the GCM temperature projections, based on level of agreement with the observed temperature record from 1961 to 2010. Their agreement criteria involved model representation of spatial and temporal patterns of climate change, found using empirical orthogonal functions and a covariance matrix analysis.

Figure 15 compares our simulation for RCP 8.5 to the 66 % confidence interval for ΔT reported by Rowlands et al. (2012) for SRES A1B. We have not adjusted for the slight differences in anthropogenic RF between RCP 8.5 and SRES A1B. We have, however, adjusted our fit criteria to $\chi^2 \leq 4$ and restricted γ to be positive, resulting in the divergence of our ΔT generally matching the Rowlands et al. (2012) divergence. The similarity of these two estimates of ΔT at the time CO_2 doubles suggests a primary reason for the dispersion reported by Rowlands et al. (2012) could be due to uncertainty in NAA RF for the contemporary atmosphere, coupled with the cantilevering of NAA RF_{2005} and γ and strong dependence of future temperature on γ. Rowlands et al. (2012) do not assign a specific cause to the dispersion of ΔT. We conclude by noting our highest estimate of ΔT at the time CO_2 doubles (Fig. 15) is a bit lower than the upper limit of Rowlands et al. (2012) and our highest estimate is achieved only for strong aerosol cooling for the contemporary atmosphere, which of course is modeled to lessen by year 2053. If γ rises over time, as may be the case for the GCM simulations shown by Rowlands et al. (2012), then actual warming could exceed the largest values from our regression shown in Fig. 15.

ACPD
12, 23913–23974, 2012

3.4 Climate sensitivity

Equilibrium climate sensitivity, $\Delta T_{2\times CO_2}$, is a complicated diagnostic because, as described in Sect. 3.2, simulations with a large fraction of anthropogenic RF of climate exported to the ocean tend to lie far from equilibrium (i.e. ΔT_{2053} for RCP 8.5 < $\Delta T_{2\times CO_2}$, as shown in Fig. 9 for 2× Gouretski) whereas simulations with a small fraction of anthropogenic RF exported to the ocean lie close to equilibrium (i.e. ΔT_{2053} for RCP 8.5 ≈ $\Delta T_{2\times CO_2}$, for Church and 0.5× Church). Equilibrium climate sensitivity versus NAA RF for the contemporary atmosphere from GCMs, using values of these parameters reported by Kiehl (2007), exhibits considerable scatter. Ocean heat export was not reported for the 9 GCMs examined by Kiehl (2007), but he did suggest differences in OHE could be responsible for the departure of a compact relation between total RF and climate sensitivity. Knutti et al. (2002) documented a strong relation between OHE and $\Delta T_{2\times CO_2}$. We find a similar dependence of these two parameters (Fig. 9a), yet our projections of ΔT out to 2060 are insensitive to OHE, as described in Sect. 3.3.

Figure 16 compares $\Delta T_{2\times CO_2}$ for the four representations of OHE used above. The data points represent $\Delta T_{2\times CO_2}$ for the best fit of the climate record, for NAA RF_{2005} = $-1.0\,W\,m^{-2}$. The error bars represent the range of $\Delta T_{2\times CO_2}$ resulting from acceptable fits to the climate record, for the empirical range of NAA RF_{2005}. Figure 16 also includes estimates of $\Delta T_{2\times CO_2}$ found from an analysis of Earth Radiation Budget Experiment (ERBE) data (Forster and Gregory, 2006), Table TS.5 of IPCC (2007), the analysis of output from 9 GCM models reported by Kiehl (2007), and another empirical model of climate described by Schwartz (2012).

Figure 16 shows that equilibrium climate sensitivity extracted from our MLR model, based on Eq. (9) and considering only export of heat to the upper 700 m of the ocean, lies on the low end of values based on GCMs, ERBE data, and another empirical model. The dependence of $\Delta T_{2\times CO_2}$ on OHE is also apparent. In our model framework, the IPCC (2007) best estimate for $\Delta T_{2\times CO_2}$ of 2.9 °C implies $\gamma = 1.6$. The sensitivity parameter γ found for best fits to the climate record, assuming only export of heat

ACPD
12, 23913–23974, 2012

to the upper 700 m of the ocean, maximizes at 1.4 for OHC = 2×Gouretski and NAA $RF_{2005} = -2.2\,W\,m^{-2}$ (Fig. 9a).

The export of heat to levels of the ocean below 700 m, hereafter the deep ocean, is the source of considerable uncertainty (e.g. Hansen et al., 2011). The associated temperature rise is very small given the mass of the deep ocean, so a long time series of stable temperature measurements is needed to define the rise in OHC of the deep ocean. Section 5.2.2.3 of IPCC (2007) states the rise in OHC, between 1961 and 2003, "accounts for more than 90 % of the possible increase in heat content of the Earth system". If so, considerable heat must be exported from the upper ocean to the deep ocean, because none of the measurements of OHC between 0 and 700 m depth show OHE anywhere close to 90 % of the atmospheric radiative perturbation (i.e. Carton and Santorelli, 2008). Hansen et al. (2011) state "most climate models mix heat too efficiently into the deep ocean" and point to measurements of OHC in the abyssal ocean (Purkey and Johnson, 2010) as evidence for this improper characteristic of GCMs.

Figure 17 is designed to show that if GCMs are indeed placing too much heat into the deep ocean and if the export of heat is a constant fraction of the anthropogenic RF of climate, then the primary consequence will be erroneous determination of equilibrium climate sensitivity. The projection of future ΔT from GCMs could be unaffected, provided feedbacks are allowed to adjust such that the past climate record is still matched. Figure 17 shows a simulation for NAA $RF_{2005} = -1.0\,W\,m^{-2}$, RCP 8.5, for which Ω (the fraction of heat exported to the ocean) has been set equal to 0.7. This results in $\gamma = 1.6$ for the best fit to the climate record (Model 5). Figure 17 shows a projection of ΔT for this model (top rung) and the inferred export of heat to the deep ocean, assuming the Gouretski and Reseghetti (2010) estimate of OHC is correct. An enormous amount of heat must be exported to depths below 700 m to obtain a climate sensitivity of 2.9 °C for a simulation constrained to match CRU4 ΔT. In our framework, γ adjusts: GHG RF needs considerable amplification to match the CRU4 data, since so much heat leaves the atmospheric component of the climate system. Provided OHE is a constant

ACPD
12, 23913–23974, 2012

fraction of the anthropogenic RF of climate, projected ΔT in year 2053 for Model 5 is very similar to projections from Models 3 and 4.

If, as suggested by Hansen et al. (2011), GCMs truly do export more heat to the deep ocean than supported by observation, our model framework suggests climate feedbacks within GCMs are likely too large. Simply reducing export of heat to the deep ocean, and allowing this energy to heat the atmosphere and ocean skin within a GCM, while retaining the high feedbacks that presently lead to $\Delta T_{2\times CO_2} \approx 2.9\,^{\circ}C$, would result in unacceptably poor simulations of past climate. On the other hand, perhaps the high climate sensitivity of GCMs results from dramatic increases in γ over time. Equilibrium climate sensitivity is a complicated diagnostic. The climate community should develop a means to account for the OHE-dependence of the gap between ΔT computed by a GCM at the time CO_2 doubles and the value of $\Delta T_{2\times CO_2}$ abstracted from GCMs, in order to make better use of this diagnostic.

We conclude by focusing on inferences of equilibrium climate sensitivity based on the response to the eruption of Mt. Pinatubo and other volcanoes. Wigley et al. (2005) examined the responses of surface temperature to the four major eruptions since 1900 and concluded the cooling associated with Mt. Pinatubo was most consistent with a climate sensitivity of ~3 °C, with a range of 1.79 to 5.21 °C. Our best fit to the 110 yr CRU4 data record, shown in Fig. 16, results in climate sensitivities below the Wigley et al. (2005) lower limit if we use OHC from Church et al. (2011) or 0.5× Church and close to the Wigley lower limit for OHC from either Gouretski and Reseghetti (2010) or 2× Gouretski.

We suggest in Canty et al. (2012) that prior neglect of the influence of variations in the strength of the AMOC on global climate has led to as much as a factor of 2 over estimate of cooling attributed to volcanoes, for the four major eruptions since 1900. The precise quantification of volcanic cooling is quite sensitive to how the AMO index is detrended and there is considerable debate regarding whether variations in the AMO index, and OHE, are a response to volcanic aerosols (e.g. Sect. 4.3 of Canty et al., 2012).

ACPD
12, 23913–23974, 2012

The nature of the perturbation to the climate system by volcanic aerosols that reach the stratosphere, especially the well documented response to Mt. Pinatubo, is dramatically different than the perturbation by GHGs. Following Pinatubo, there was a large increase in reflected solar radiation (particularly in the tropics), a significant rise in trapped thermal radiation due to absorption and re-emission of heat by the volcanic aerosols (particularly in the extra-tropics), and a large increase in tropical lower stratosphere upwelling (e.g. Sect. 5.1 of Canty et al., 2012). Rising GHGs trap and re-emit heat throughout the atmospheric column and, as a result, changes the lapse rate in a manner that almost certainly acts as a negative feedback that partially offsets the positive water vapor feedback (Fig. 8.14 of IPCC, 2007). If the suggestion raised by Canty et al. (2012) that volcanic cooling has been over estimated is shown to be incorrect, we still question the applicability of volcanically-inferred climate sensitivity to the evaluation of long-term climate simulations by GCMs, because the physical nature of the forcings by GHGs and volcanic aerosols are so different. Inferences of climate sensitivity from the long-term climate record, such as those shown in Fig. 16, may offer a more appropriate test for the representation of feedbacks within GCMs.

4 Discussion

We have shown that the near monotonic rise of the global average surface temperature anomaly (ΔT) from 1900 to 2010 is clearly associated with anthropogenic radiative forcing of climate (AF). Nonetheless, future climate is inherently uncertain because past climate can be fit, in an acceptable manner, by a wide range of combinations of values for γ (feedback in response to a GHG RF perturbation), net anthropogenic aerosol radiative forcing for the contemporary atmosphere (NAA RF_{2005}), and ocean heat export (OHE). In our model framework, where γ is allowed to adjust to prescribed NAA RF_{2005} and OHE, and the fraction of AF exported to the ocean is assumed to stay constant over time, future ΔT is shown to depend primarily on NAA RF and γ. Reduced uncertainty for projections of future climate likely requires external, observationally

ACPD
12, 23913–23974, 2012

based constraints with sufficient accuracy and precision to narrow the uncertainties that presently exist for NAA RF and γ. Here, we offer a brief discussion of the literature on NAA RF and γ.

Despite the publication of hundreds if not thousands of papers on atmospheric aerosols since IPCC (2007), few focus on empirical determination of NAA RF. Morgan et al. (2006) published an overview and concluded "all best estimates of total aerosol [radiative] forcing were negative, with values ranging between $-0.25\,W\,m^{-2}$ and $-2.1\,W\,m^{-2}$", which is quite consistent with the range of NAA RF_{2005} considered in Sect. 3. Kahn (2011) has published a comprehensive overview of direct RF due to aerosols, but the total RF due to aerosols is likely much larger (e.g. Storelvmo et al., 2009).

Murphy et al. (2009) estimated NAA RF from the mid 1950s to 2001 based on an analysis of Earth's energy balance that relies on measurements from Earth Radiation Budget Experiment (ERBE) instruments and observations of ocean heat content (OHC). Murphy et al. (2009) concluded NAA RF averaged $-1.1 \pm 0.4\,W\,m^{-2}$ between 1970 and 2000 and recently approached $-1.7\,W\,m^{-2}$. Their recent rise in aerosol cooling is hard to understand because sulfur emissions have been declining since about 1980, leading to time series of NAA RF, such as those shown in Fig. 3, which should have slowly varying cooling peaks. Murphy et al. (2009) used the Domingues et al. (2008) measurement of OHC and do not consider export of heat to depths of the ocean below 700 m. Had they used the OHC record of Gouretski and Reseghetti (2010), their estimate of NAA RF cooling would likely be weaker for later years than shown in their Fig. 4, due to large difference in OHE inferred from data provided by the group of Domingues et al. (2008) and Gouretski and Reseghetti (2010). Proper determination of NAA RF is dependent on accurate quantification of OHC.

Hansen et al. (2011) conducted an analysis of Earth's energy budget and concluded NAA RF for the contemporary atmosphere is $-1.6 \pm 0.3\,W\,m^{-2}$. If a consensus emerges from the next IPCC report that NAA RF can truly be constrained as well as Hansen et al. (2011) suggest, then future uncertainty in projected climate will be reduced but

ACPD
12, 23913–23974, 2012

not eliminated, because many values of the γ can yield an acceptable fit to the climate record, even if NAA RF is precisely known. As described in Sect. 14.6.2 of Hansen et al. (2011), the launch failure of the National Aeronautics and Space Administration (NASA) Glory mission was a tremendous setback to progressing on direct, empirical determination of NAA RF.

While it is tempting to relate our values of the sensitivity parameter γ to the literature on the values of feedbacks involving water vapor, lapse rate, surface albedo, and clouds, we will rely instead on IPCC (2007) and only a handful of papers. As described in Sect. 8.6 of IPCC (2007), there is a strong consensus that the water vapor feedback is positive and that this feedback is offset to a considerable extent by the negative lapse rate feedback. Examination of the components of our sensitivity parameter γ using Eq. (3) and values for $\gamma_{\text{WATER VAPOR}}$ and $\gamma_{\text{LAPSE RATE}}$ abstracted from Chap. 8 of IPCC (2007) leads us to conclude that for most of our regressions the net affect of clouds and surface albedo would have to constitute a negative feedback to GHG RF of climate. Within GCMs there is no consensus regarding the sign of the cloud feedback (e.g. Fig. 10.5 of IPCC, 2007). A recent analysis of cloud height fluctuations measured by the NASA Multi-angle Imaging SpectroRadiometer provides empirical support for a negative feedback to GHG RF from clouds (Davies and Malloy, 2012). But this study extends for only 10 yr and, as the authors state, ten years is too short for any definitive conclusion because "the linear trend in global cloud height of -44 ± 22 m over the last decade is partly influenced by the La Niña event, and may prove ephemeral."

Reduction in the uncertainty of γ will also require precise, empirical determination of Earth's surface albedo. GCMs consider surface albedo to be a positive feedback on climate (Fig. 8.14 of IPCC, 2007); as GHGs rise, albedo declines, due mainly to loss of snow and sea ice. Measurements of terrestrial radiation reflected from the moon (earthshine), together with an analysis of albedo inferred from the International Satellite and Cloud Climatology Project, suggest a steady decline in Earth's albedo from 1985 to 2000, followed by a recent, sudden rise that is difficult to understand (Goode and Pallé, 2007). However, an examination of NASA Clouds and the Earth's Radiant

ACPD
12, 23913–23974, 2012

Energy System data by Wielicki et al. (2005) finds changes in albedo that contradict the earthshine record. Reaching consensus on the contribution of surface albedo to γ is a daunting challenge that may be not be met until the entire disk of the Earth can be monitored from a stable, space-based vantage point.

5 Conclusions

We have used an empirical model of climate to show that measurements of the global mean surface temperature anomaly (ΔT) over the past 110 yr can be fit well for a set of compact, well defined relations between γ (sensitivity parameter for response of climate to a GHG RF perturbation) and NAA RF_{2005} (net anthropogenic aerosol RF including feedbacks for the contemporary atmosphere). The specific relation is dependent on ocean heat export.

Over the next four decades, the RF perturbation to GHGs is projected to rise, perhaps steeply, whereas the RF due to anthropogenic aerosols is projected to slowly decline due to air quality regulations. Even if we assume that whatever climate feedback has operated over the past 110 yr persists for another 40 yr (i.e. the value of γ inferred from the climate record remains constant), future climate is inherently difficult to project because there is a wide range of possible combinations of aerosol radiative forcing and γ that provide acceptable fits to the climate record. One possibility is that aerosols exert small cooling on present day global climate, in which case climate feedback must be moderate and the future rise in global average surface temperature at the time CO_2 doubles could be less than ~1.0 °C. On the other hand, if aerosols exert large contemporary cooling on global climate, feedback must be large and the future rise in global average surface temperature at the time CO_2 doubles could be as high as ~2.2 °C. An empirical determination of NAA RF (Murphy et al., 2009) and a recent analysis of Earth's energy budget (Hansen et al., 2011) both suggest aerosols exert a large contemporary cooling, despite recent declines in sulfur emissions over Asia (Li et al., 2010) and globally (Smith et al., 2011). If this is the case, the higher estimate of

ACPD
12, 23913–23974, 2012

future warming is more likely. We reiterate our projected future temperature increases are found assuming no change in climate feedback, which involves a myriad of processes affecting atmospheric water vapor, lapse rate, clouds, and surface albedo, and hence should be treated with considerable caution.

If our model framework is at all applicable to GCMs, then use of the equilibrium climate sensitivity from GCMs is complicated. Equilibrium climate sensitivity denotes the rise in global surface temperature after the climate system has attained a new equilibrium in response to a doubling of atmospheric CO_2. We show that under conditions of small ocean heat export, the modeled rise in temperature at the time CO_2 doubles is close to the equilibrium climate sensitivity. When ocean heat export is large, the modeled rise in temperature at the time CO_2 doubles is much smaller than the equilibrium climate sensitivity.

There are two emerging issues regarding ocean heat export. GCMs may be exporting larger amounts of heat to ocean depths below 700 m than measured (Hansen et al., 2011). If so, this could explain why the IPCC (2007) GCMs exhibit larger equilibrium climate sensitivity then suggested by our analysis of the climate record. Two recent measurements of ocean heat content (OHC) of the upper 700 m of the ocean, from which ocean heat export (OHE) is inferred, provide contrasting views. The OHC measurements of Church et al. (2011) are consistent with export of only ~20 % of the anthropogenic RF of climate to the upper ocean, whereas the OHC measurements of Gouretski and Reseghetti (2010) imply export of ~37 % of the anthropogenic RF to the upper ocean. Provided the export of heat to the world's oceans is a constant fraction of the anthropogenic RF perturbation and also climate feedbacks are allowed to adjust in response to prescribed OHE, our simulations show projected future temperature is insensitive to OHE. However, equilibrium climate sensitivity is dependent on OHE and many analyses of Earth's energy budget, used for example to infer NAA RF (Murphy et al., 2009) or climate sensitivity (Forster and Gregory, 2006), require accurate determination of OHE.

ACPD
12, 23913–23974, 2012

Supplementary material related to this article is available online at: http://www.atmos-chem-phys-discuss.net/12/23913/2012/acpd-12-23913-2012-supplement.pdf.

Acknowledgements. We appreciate helpful email exchanges with John Daniel, Jim Elkins, Jean-Francois Lamarque, Judith Lean, Malte Meinshausen, Steven Montzka, David Stern, Guus Velders, and Thomas Wigley at various stages of this study. Comments from colleagues at the 2011 Santa Fe Conference on Global and Regional Climate Change are also appreciated.

References

Canty, T., Mascioli, N. R., Smarte, M., and Salawitch, R. J.: An empirical model of global climate – Part 1: Reduced impact of volcanoes upon consideration of ocean circulation, Atmos. Chem. Phys. Discuss., 12, 23829–23911, doi:10.5194/acpd-12-23829-2012, 2012.

Carton, J. A. and Santorelli, A.: Global upper ocean heat content as viewed in nine analyses, J. Clim., 21, 6015–6035, doi:10.1175/2008JCLI2489.1, 2008.

Church, J. A., White, N. J., Konikow, L. F., Domingues, C. M., Cogley, J. G., Rignot, E., Gregory, J. M., van den Broecke, M. R., Monaghan, A. J., and Velicogna, I.: Revisiting the Earth's sea-level and energy budgets from 1961 to 2008, Geophys. Res. Lett., 38, L18601, doi:10.1029/2011GL048794, 2011.

Davies, R. and Molloy, M.: Global cloud height fluctuations measured by MISR on Terra from 2000 to 2010, Geophys. Res. Lett., 39, L03701, doi:10.1029/2011GL050506, 2012.

Domingues, C. M., Church, J. A., White, N. J., Glecker, P. J., Wijffels, S. E., Barker, P. M., and Dunn, J. R.: Improved estimates of upper-ocean warming and multidecadal sea-level rise, Nature, 453, 1090–1093, doi:10.1038/nature07080, 2008.

Enfield, D. B., Mestas-Nuñez, A. M., and Trimble, P. J.: The Atlantic Multidecadal Oscillation and its relation to rainfall and river flows in the continental US, Geophys. Res. Lett. 28, 2077–2080, doi:10.1029/2000GL012745, 2001.

Forster, P. M. D. and Gregory, J. M.: The climate sensitivity and its components diagnosed from Earth Radiation Budget data, J. Clim., 19, 39–52, doi:10.1175/JCLI3611.1, 2006.

ACPD

12, 23913–23974, 2012

Goode, P. R. and Pallé, E.: Shortwave forcing of the Earth's climate: modern and historical variations in the Sun's irradiance and the Earth's reflectance, J. Atmos. Sol.-Terr. Phy., 69, 1556–1568, 2007.

Gouretski, V. and Reseghetti, F.: On depth and temperature biases in bathythermograph data: development of a new correction scheme based on analysis of a global ocean database, Deep-Sea Res. Pt. I, 57, 812–833, doi:10.1016/j.dsr.2010.03.011, 2010.

Hansen, J. E., Lacis, A., Rind, D., Russell, G., Stone, P., Fung, I., Ruedy, K., and Lerner, J.: Climate sensitivity: analysis of feedback mechanisms, Amer. Geophys. Union, Monogr. Ser., 29, 130–163, 1984.

Hansen, J., Sato, M., Kharecha, P., and von Schuckmann, K.: Earth's energy imbalance and implications, Atmos. Chem. Phys., 11, 13421–13449, doi:10.5194/acp-11-13421-2011, 2011.

IPCC, 2001: Climate Change 2001: The Scientific Basis. Contribution of Working Group I to the Third Assessment Report of the Intergovernmental Panel on Climate Change, edited by: Houghton, J. T., Ding, Y., Griggs, D. J., Noguer, M., van der Linden, P. J., Dai, X., Maskell, K., and Johnson, C. A., Cambridge University Press, Cambridge, UK and New York, NY, USA, 881 pp., 2001.

IPCC, 2007: Climate Change 2007: The Physical Science Basis. Contribution of Working Group I to the Fourth Assessment Report of the Intergovernmental Panel on Climate Change, edited by: Solomon, S., Qin, D., Manning, M., Chen, Z., Marquis, M., Averyt, K. B., Tignor, M., and Miller, H. L., Cambridge University Press, Cambridge, UK and New York, NY, USA, 996 pp., 2007.

Jones, P. D., Lister, D. H., Osborn, T. J., Harpham C., Salmon, M., and Morice, C. P.: Hemispheric and large-scale land-surface air temperature variations: an extensive revision and an update to 2010, J. Geophys. Res., 117, D05127, doi:10.1029/2011JD017139, 2012.

Kahn, R.: Reducing the uncertainties in direct aerosol radiative forcing, Surveys in Geophysics, 33, 701–721, doi:10.1007/s10712-011-9153-z, 2012.

Kennedy, J. J., Rayner, N. A., Smith, R. O., Saunby, M., and Parker, D. E.: Reassessing biases and other uncertainties in sea-surface temperature observations since 1850, Part 1: Measurement and sampling errors, J. Geophys. Res., 116, D14103, doi:10.1029/2010JD015218, 2011a.

Kennedy, J. J., Rayner, N. A., Smith, R. O., Saunby, M. and Parker, D. E.: Reassessing biases and other uncertainties in sea-surface temperature observations since 1850, Part 2: Biases and homogenization, J. Geophys. Res., 116, D14104, doi:10.1029/2010JD015220, 2011b.

ACPD

12, 23913–23974, 2012

Kiehl, J. T.: Twentieth century climate model response and climate sensitivity, Geophys. Res. Lett., 34, L22710, doi:10.1029/2007GL031383, 2007.
Knight J. R., Allan, R. J., Folland, C. K., Vellinga, M., and Mann, M. E.: A signature of persistent natural thermohaline circulation cycles in observed climate, Geophys. Res. Lett., 32, L20708, doi:10.1029/2005GL024233, 2005.
Knutti, R. and Hegerl, G. C.: The equilibrium sensitivity of the Earth's temperature to radiation changes, Nature Geosci., 1, 735–743, doi:10.1038/ngeo337, 2008.
Knutti, R., Stocker, T. F., Joos, F., and Plattner, G.-K.: Constraints on radiative forcing and future climate change from observations and climate model ensembles, Nature, 416, 719–723, doi:10.1038/416719a, 2002.
Knutti, R., Furrer, R., Tebaldi, C., Cermak, J., and Meehl, G. A.: Challenges in combining projections from multiple climate models, J. Clim., 23, 2739–2758, doi:10.1175/2009JCLI3361.1, 2010.
Lean, J. L.: Evolution of the Sun's spectral irradiance since the Maunder minimum, Geophys. Res. Lett., 27, 2425–2428, doi:10.1029/2000GL000043, 2000.
Lean, J. L. and Rind, D. H.: How will Earth's surface temperature change in future decades?, Geophys. Res. Lett., 36, L15708, doi:10.1029/2009GL038932, 2009.
Li, C., Zhang, Q., Krotkov, N. A., Streets, D. G., He, K., Tsay, S.-C., and Gleason, J. F.: Recent large reduction in sulfur dioxide emissions from Chinese power plants observed by the Ozone Monitoring Instrument, Geophys. Res. Lett., 37, L08807, doi:10.1029/2010GL042594, 2010.
Masui, T., Matsumoto, K., Hijioka, Y., Kinoshita, T., Nozawa, T., Ishiwatari, S., Kato, E., Shukla, P. R., Yamagata, Y., and Kainuma, M.: An emission pathway for stabilization at 6 $W m^{-2}$ radiative forcing, Climatic Change, 109, 59–76, doi:10.1007/s10584-011-0150-5, 2011.
Matthews, H. D. and Zickfeld, K.: Climate response to zeroed emissions of greenhouse gases and aerosols, Nature Clim. Change, 2, 338–341, doi:10.1038/nclimate1424, 2012.
Medhaug, I. and Furevik, T.: North Atlantic 20th century multidecadal variability in coupled climate models: sea surface temperature and ocean overturning circulation, Ocean Sci., 7, 389–404, doi:10.5194/os-7-389-2011, 2011.
Meinshausen, M., Smith, S. J., Calvin, K. V., Daniel, J. S., Kainuma, M. L. T., Lamarque, J.-F., K Matsumoto, K., Montzka, S., Raper, S., Riahi, K., Thomson, A. M., Velders, G. J. M., and van Vuuren, D. P.: The RCP greenhouse gas concentrations and their extensions from 1765 to 2300, Climatic Change, 109, 213–241, doi:10.1007/s10584-011-0156-z, 2011.

ACPD
12, 23913–23974, 2012

Morgan, M. G., Adams, P. J., and Keith, D. W.: Elicitation of expert judgments of aerosol forcing, Climatic Change, 75, 195–214, doi:10.1007/s10584-005-9025-y, 2006.
Morice, C. P., Kennedy, J. J., Rayner, N. A., and Jones, P. D.: Quantifying uncertainties in global and regional temperature change using an ensemble of observational estimates: the HadCRUT4 data set, J. Geophys. Res., 117, D08101, doi:10.1029/2011JD017187, 2012.
Murphy, D. M., Solomon, S., Portmann, R. W., Rosenlof, K. H., Forster, P. M., and Wong, T.: An observationally based energy balance for the Earth since 1950, J. Geophys. Res., 114, D17107, doi:10.1029/2009JD012105, 2009.
Myhre, G., Highwood, E. J., Shine, K. P., and Stordal, F.: New estimates of radiative forcing due to well mixed greenhouse gases, Geophys. Res. Lett., 25, 2715–2718, doi:10.1029/98GL01908, 1998.
Myhre, G., Myhre, A., and Stordal, F.: Historical evolution of radiative forcing of climate, Atmos. Env., 35, 2361–2373, doi:10.1016/S1352-2310(00)00531-8, 2001.
Purkey, S. G. and Johnson, G. C.: Warming of global abyssal and deep southern ocean waters between the 1990s and 2000s: contributions to global heat and sea level rise budgets, J. Clim., 23, 6336–6351, doi:10.1175/2010JCLI3682.1, 2010.
Riahi, K., Grüber, A., and Nakicenovic, N.: Scenarios of long-term socio-economic and environmental development under climate stabilization, Technol. Forecast. Soc. Change, 74, 887–935, doi:10.1016/j.techfore.2006.05.026, 2007.
Riahi, K., Rao, S., Krey, V., Cho, C., Chirkov, V., Fischer, G., Kindermann, G., Nakicenovic, N., and Rafaj, P.: RCP 8.5 – a scenario of comparatively high greenhouse gas emissions, Climatic Change, 109, 33–57, doi:10.1007/s10584-011-0149-y, 2011.
Rohde, R., Curry, J., Groom, D., Jacobsen, R., Muller, R. A., Perlmutter, S., Rosenfeld, A., Wickham, C., and Wurtele, J.: Berkeley Earth temperature averaging process, J. Geophys Res., available at: http://berkeleyearth.org/available-resources, submitted, 2011.
Rowlands, D. J., Frame, D. J., Ackerley, D., Aina, T., Booth, B. B. B., Christensen, C., Collins, M., Faull, N., Forest, C. E., Grandey, B. S., Gryspeerdt, E., Highwood, E. J., Ingram, W. J., Knight, S., Lopez, A., Massey, N., McNamara, F., Meinshausen, N., Piani, C., Rosier, S. M., Sanderson, B. M., Smith, L. A., Stone, D. A., Thurston, M., Yamazaki, K., Yamazaki, Y. H., and Allen, M. R.: Broad range of 2050 warming from an observationally constrained large climate model ensemble, Nature Geosci., 5, 256–260, doi:10.1038/NGEO1430, 2012.
Saji, H. H., Goswami, B. N., Vinayachandran, P. H., and Yamagata, T.: A dipole mode in the tropical Indian Ocean, Nature, 401, 360–363, doi:10.1038/43854, 1999.

ACPD
12, 23913–23974, 2012

Sato, M., Hansen, J. E., McCormick, M. P., and Pollack, J. B.: Stratospheric aerosol optical depths, 1850–1990, J. Geophys. Res., 98, 22987–22994, doi:10.1029/93JD02553, 1993.

Schlesinger, M. E. and Ramankutty, N.: An oscillation in the global climate system of period 65–70 years, Nature, 367, 723–726, doi:10.1038/367723a0, 1994.

Schwartz, S. E., Charlson, R. J., Kahn, R. A., Ogren, J. A., and Rodhe, H.: Why hasn't Earth warmed as much as expected?, J. Clim., 23, 2453–2464, doi:10.1175/2009JCLI3461.1, 2007.

Schwartz, S. E.: Determination of Earth's transient and equilibrium climate sensitivities from observations over the twentieth century: strong dependence on assumed forcing, Surv. Geophys., 33, 745–777, doi:10.1007/s10712-012-9180-4, 2012.

Smith, S. J., van Aardenne, J., Klimont, Z., Andres, R. J., Volke, A., and Delgado Arias, S.: Anthropogenic sulfur dioxide emissions: 1850–2005, Atmos. Chem. Phys., 11, 1101–1116, doi:10.5194/acp-11-1101-2011, 2011.

Stern, D. I.: An atmosphere-ocean time series model of global climate change, Comput. Stat. Data An., 51, 1330–1346, doi:10.1016/j.csda.2005.09.016, 2006a.

Stern, D. I.: Reversal of the trend in global anthropogenic sulfur emissions, Chemosphere, 16, 207–220, doi:10.1016/j.gloenvcha.2006.01.001, 2006b.

Storelvmo, T., Lohmann, U., and Bennartz, R.: What governs the spread in shortwave forcings in the transient IPCC AR4 models?, Geophys. Res. Lett., 36, L01806, doi:10.1029/2008GL036069, 2009.

Stott, P. A. and Forest, C. E.: Ensemble climate predictions using climate models and observational constraints, Phil. Trans. R. Soc. A, 365, 2029–2052, doi:10.1098/rsta.2007.2075, 2007.

Stouffer, R. J., Yin, J., Gregory, J. M., Dixon, K. W., Spelman, M. J., Hurlin, W., Weaver, A. J., Eby, M., Flato, G. M., Hasumi, H., Hu, A., Jungclaus, J. H., Kamenkovich, I. V., Levermann, A., Montoya, M., Murakami, S., 5 Nawrath, S., Oka, A., Peltier, W. R., Robitaille, D. Y., Sokolov, A., Vettoretti, G., and Webber, S. L.: Investigating the causes of the response of the thermohaline circulation to past and future climate changes, J. Clim., 19, 1365–1387, doi:10.1175/JCLI3689.1, 2006.

Thompson, D. W. J., Kennedy, J. J., Wallace, J. M., and Jones, P. D.: A large discontinuity in the mid-twentieth century in observed global-mean surface temperature, Nature, 453, 646–649, doi:10.1038/nature06982, 2008.

ACPD

12, 23913–23974, 2012

Thomson, A. M., Calvin, K. V., Smith, S. J., Kyle, G. P., Volke, A., Patel, P., Delgado-Arias, S., Bond-Lamberty, B., Wise, M. A., Clarke, L. E., and Edmonds, J. A.: RCP4.5: a pathway for stabilization of radiative forcing by 2100, Climatic Change, 109, 77–94, doi:10.1007/s10584-011-0151-4, 2011.

Trenberth, K. E. and Shea, D. J.: Atlantic hurricanes and natural variability in 2005, Geophys. Res. Lett., 33, L12704, doi:10.1029/2006GL026894, 2006.

van Vuuren, D. P., Edmonds, J. A., Kainuma, M., Riahi, K., Thomson, A. M., Hibbard, K., Hurtt, G. C., Kram, T., Krey, V., Lamarque, J.-F., Masui, T., Meinshausen, M., Nakicenovic, N., Smith, S. J., and Rose, S.: The representative concentration pathways: an overview, Climatic Change, 109: 5–31, doi:10.1007/s10584-011-0148-z, 2011a.

van Vuuren, D. P., Stehfest, E., den Elzen, M. G. J., Kram, T., van Vliet, J., Deetman, S., Isaac, M., Goldewijk, K. K., Hof, A., Beltran, A. M., Oostenrijk, R., and van Ruijven, B.: RCP2.6: exploring the possibility to keep global mean temperature increase below 2 °C, Climatic Change, 109, 95–116, doi:10.1007/s10584-011-0152-3, 2011b.

Velders, G. J. M., Fahey, D. W., Daniel, J. S., McFarland, M., and Andersen, S. O.: The large contribution of projected HFC emissions to future climate forcing, Proc. Natl. Acad. Sci. USA, 106, 10949–10954, 2009.

Wang, Y. M., Lean, J. L., and Sheeley Jr., N. R.: Modeling the Sun's magnetic field and irradiance since 1713, Astrophys. J., 625, 522–538, doi:10.1086/429689, 2005.

Wielicki, B. A., Wong, T., Loeb, Minnis, P., Priestley, K., and Kandel, R.: Changes in Earth's albedo measured by satellite, Science, 308, 825, doi:10.1126/science.1106484, 2005.

Willis, D. K.: Can in situ floats and satellite altimeters detect long-term changes in Atlantic Ocean overturning?, Geophys. Res. Lett., 37, L06602, doi:10.1029/2010GL042372, 2010.

Wolter, K. and Timlin, M. S.: El Niño/Southern Oscillation behaviour since 1871 as diagnosed in an extended multivariate ENSO index (MEI.ext), Int. J. Climatol., 31, 1074–1087, doi:10.1002/joc.2336, 2011.

WMO (World Meteorological Organization): Scientific Assessment of Ozone Depletion: 2010, Global Ozone Research and Monitoring Project, Report # 52, Geneva, 2011.

Zhang, R., Delworth, T. L., and Held, I. M.: Can the Atlantic Ocean drive the observed multidecadal variability in Northern Hemisphere mean temperature?, Geophys. Res. Lett., 34, L02709, doi:10.1029/2006GL028683, 2007.

Zhang, Y., Wallace, J. M. and Battisti, D. S.: ENSO-like interdecadal variability: 1900–93, J. Clim., 10, 1004–1020, doi:10.1175/1520-0442(1997)010<1004:ELIV>2.0.CO;2, 1997.

ACPD
12, 23913–23974, 2012

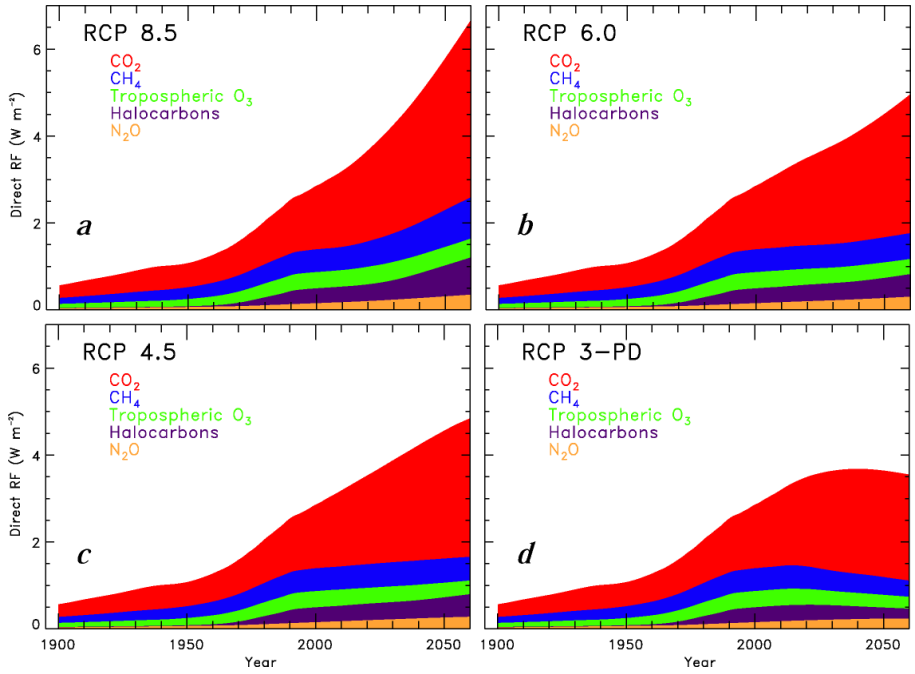

Fig. 1. Direct RF due to greenhouse gases (GHG RF) used as input for all model calculations. The colored regions show individual contributions from CO_2 (red), CH_4 (blue), tropospheric O_3 (green), halocarbons (purple), and N_2O (gold), based on global, annual mixing ratios from the four RCP scenarios, as indicated.

ACPD
12, 23913–23974, 2012

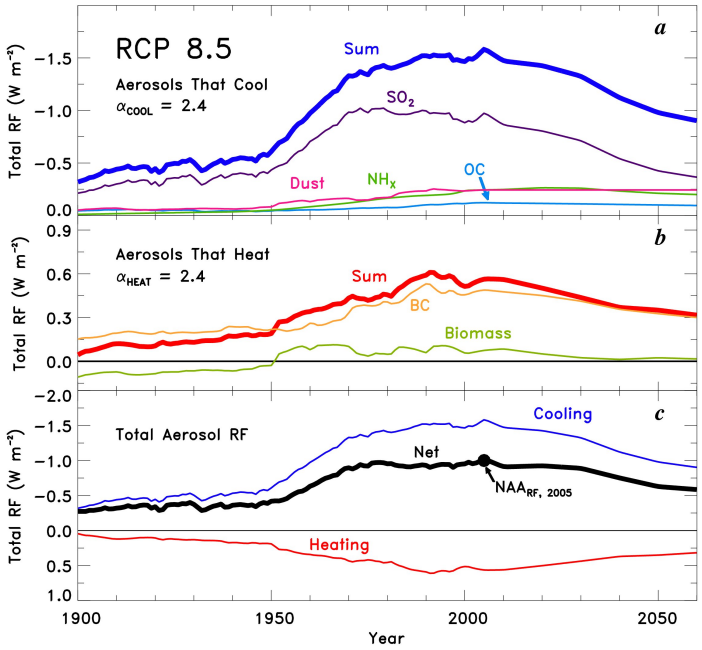

Fig. 2. (a) Total RF of tropospheric aerosols that cool, as labeled, based on our estimate of $RF_{SULATE\text{-}DIR}$ and RCP 8.5 estimates of direct RF for other components, all multiplied by α_{COOL} = 2.4, chosen so that total RF due to sulfate aerosols in 2005 equals $-0.96\,W\,m^{-2}$. The curve labeled Sum denotes total RF due to aerosols that cool. **(b)** Same as **(a)**, except for aerosols that heat. Direct RF components, from RCP 8.5, have been multiplied by α_{HEAT} = 2.4, chosen so that net anthropogenic aerosol RF (NAA RF) in year 2005 equals $-1.0\,W\,m^{-2}$ (IPCC, 2007). The curve labeled Biomass refers to emissions of OC and BC due to biomass burning, and the curves labeled OC and BC refer to fossil fuel burning emissions of these components. **(c)** Total RF of aerosols that cool (blue, α_{COOL} = 2.4), of aerosol that heat (red, α_{HEAT} = 2.4), and their sum that defines NAA RF (black curve). The value of NAA RF in year 2005 is marked.

ACPD
12, 23913–23974, 2012

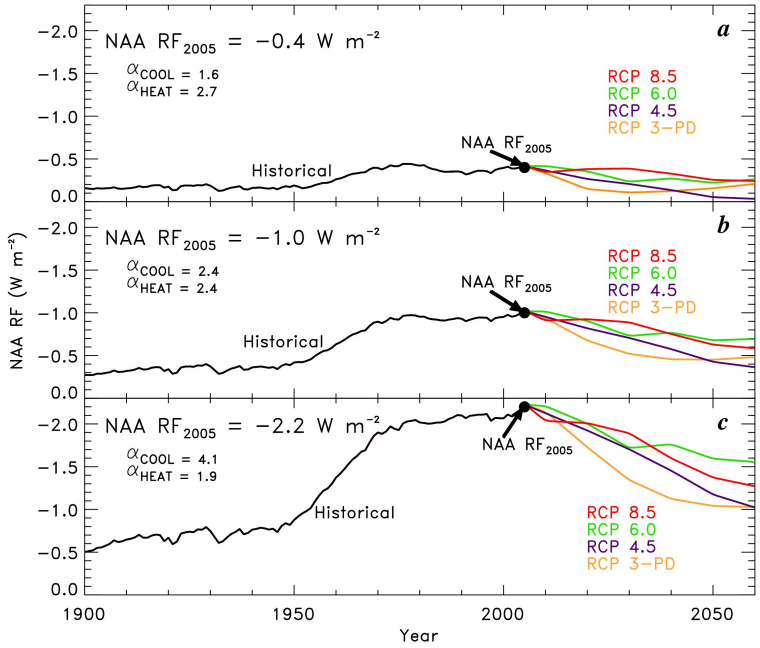

Fig. 3. (a) Net anthropogenic aerosol RF (NAA RF) from 1900 to 2060 for three scenarios: **(a)** NAA $RF_{2005} = -0.4\,W\,m^{-2}$, the least amount of aerosol cooling for the contemporary atmosphere according to our analysis of Table 2.12 of IPCC (2007), found for $\alpha_{COOL} = 1.6$ and $\alpha_{HEAT} = 2.7$; **(b)** NAA $RF_{2005} = -1.0\,W\,m^{-2}$, the best estimate of aerosol cooling for the contemporary atmosphere according to IPCC (2007), found for $\alpha_{COOL} = 2.4$ and $\alpha_{HEAT} = 2.4$; **(c)** NAA $RF_{2005} = -2.2\,W\,m^{-2}$, the largest amount of aerosol cooling for the contemporary atmosphere according to IPCC (2007), found for $\alpha_{COOL} = 4.1$ and $\alpha_{HEAT} = 1.9$. Estimates of direct RF from various components of aerosols, provided by the Potsdam Institute for Climate Impact Research (Appendix B of Canty et al., 2012) and our internal estimate of historical direct RF from sulfate aerosols (Fig. 2 of Canty et al., 2012) have been multiplied by the scaling parameters to arrive at depicted curves.

ACPD
12, 23913–23974, 2012

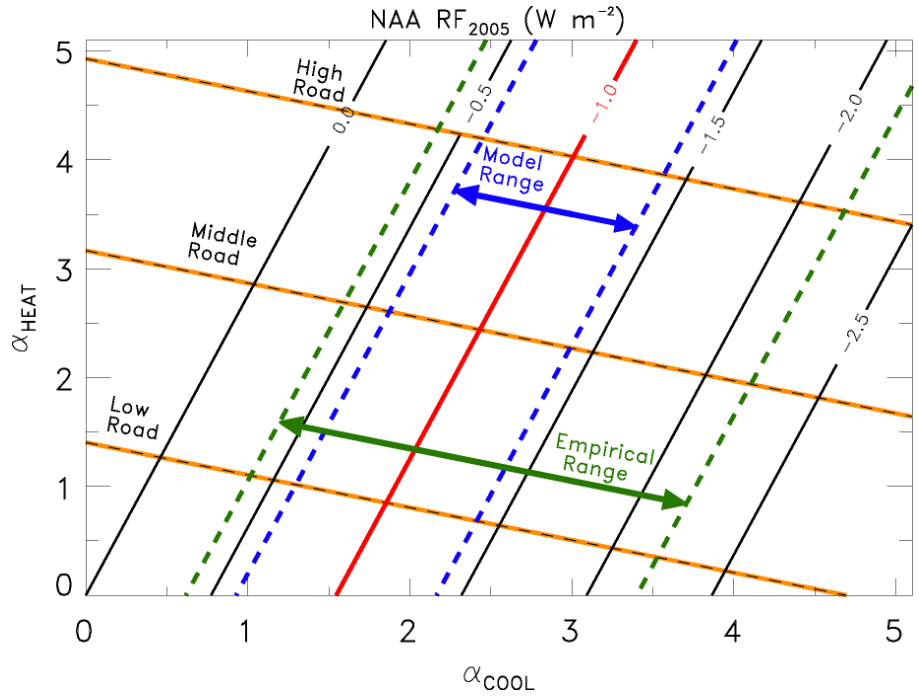

Fig. 4. Contours of net anthropogenic aerosol RF in year 2005 (NAA RF_{2005}) (black solid lines) as a function of α_{COOL} and α_{HEAT}, scaling parameters used to relate direct RF of aerosols to total RF. The contour for NAA $RF_{2005} = -1.0\,W\,m^{-2}$, the best estimate from IPCC (2007), is shown in red. The dashed green lines denote the "Empirical Range" of NAA RF_{2005} inferred from data analyses given in Table 2.12 of IPCC (2007). The dashed blue lines denote the "Model Range" of NAA RF_{2005}, based on values of this quantity from 9 GCMs reported by Kiehl (2007). The black dashed/yellow highlight lines denote various manners in which the scaling parameters α_{COOL} and α_{HEAT} can be combined to provide a particular value of NAA RF_{2005}.

ACPD
12, 23913–23974, 2012

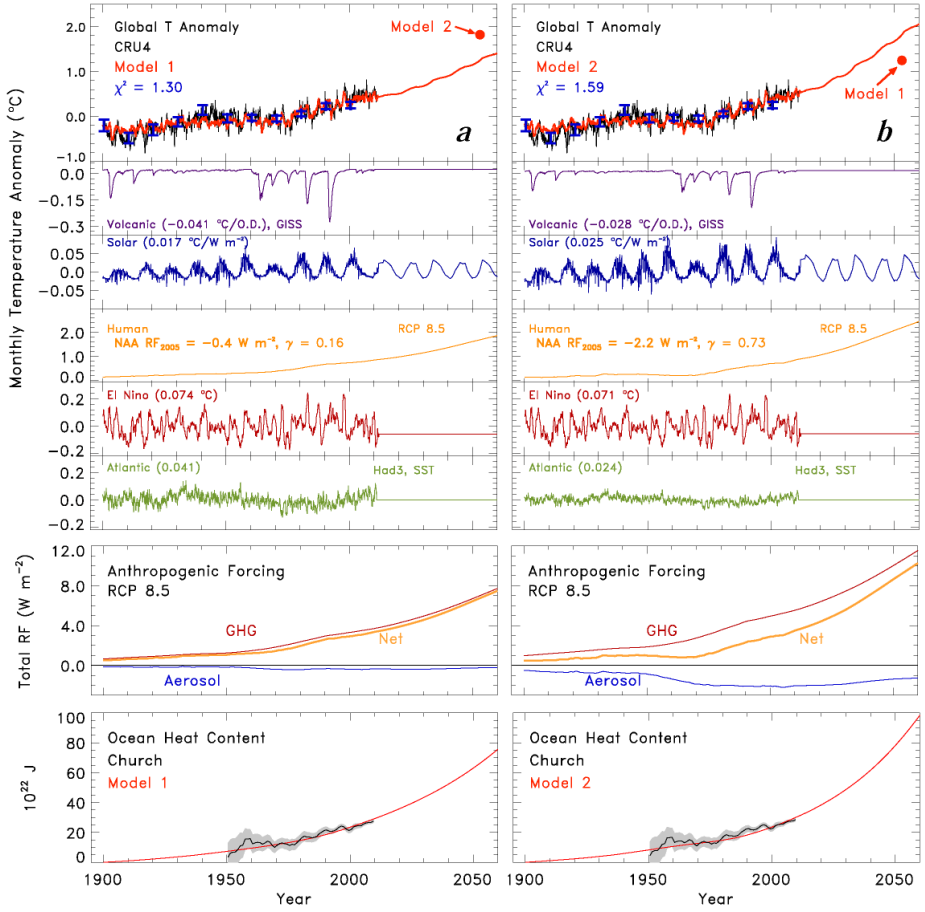

ACPD
12, 23913–23974, 2012

An empirical model of global climate – Part 2

N. R. Mascioli et al.

Fig. 5. Ladder plots showing "best fit" regressions and projections of the global temperature anomaly (ΔT), for RCP 8.5. All anomalies are with respect to the 1961 to 1990 mean. The top rung of each ladder plot shows CRU4 measured (black) and modeled (red) ΔT, from the start of 1900 to end of 2010, and projected ΔT to year 2060. Ladder plot **(a)** shows results for NAA $RF_{2005} = -0.4\,W\,m^{-2}$ the least amount of aerosol cooling (Model 1); ladder plot **(b)** shows results for NAA $RF_{2005} = -2.2\,W\,m^{-2}$, the largest amount of aerosol cooling (Model 2). The temperature anomaly in year 2053 from the other model is shown on the top rung. Values of χ^2 are given and 1-sigma uncertainty of ΔT, available for every month, is shown periodically (blue error bars). The other rungs show contributions to ΔT from Volcanoes (based on SOD), Solar (based on TSI), Humans (sum of GHG and aerosols), ENSO, and the AMO. Values of the regression coefficients are given. Specified value of NAA RF_{2005} and output value of the sensitivity parameter γ are given in the Human rung. The Anthropogenic Forcing rung shows $(1+\gamma)$ (GHG RF) (red), NAA RF (blue), and Net RF (gold). The last rung compares modeled and measured Ocean Heat Content, for runs constrained by the OHC measurement of Church et al. (2011), with all measures of OHC represented as an anomaly with respect to January 1900 (start of model run). The best fit value of γ based on regression of the historical temperature record has been found; this value of γ is used for the projection of ΔT.

ACPD
12, 23913–23974, 2012

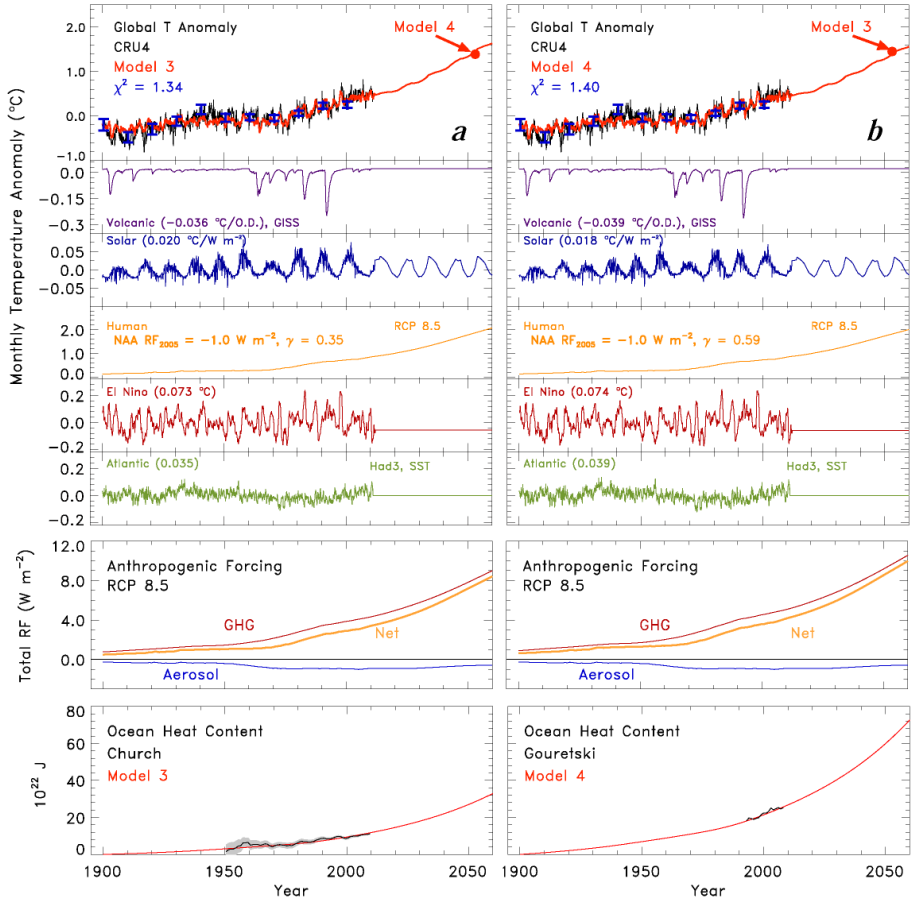

Fig. 6. Same as Fig. 5 except for NAA $RF_{2005} = -1.0\,W\,m^{-2}$, the IPCC (2007) best estimate of aerosol cooling. **(a)** Model constrained to match OHC measurement of Church et al. (2011). **(b)** Model constrained to match OHC measurement of Gouretski and Reseghetti (2010).

ACPD
12, 23913–23974, 2012

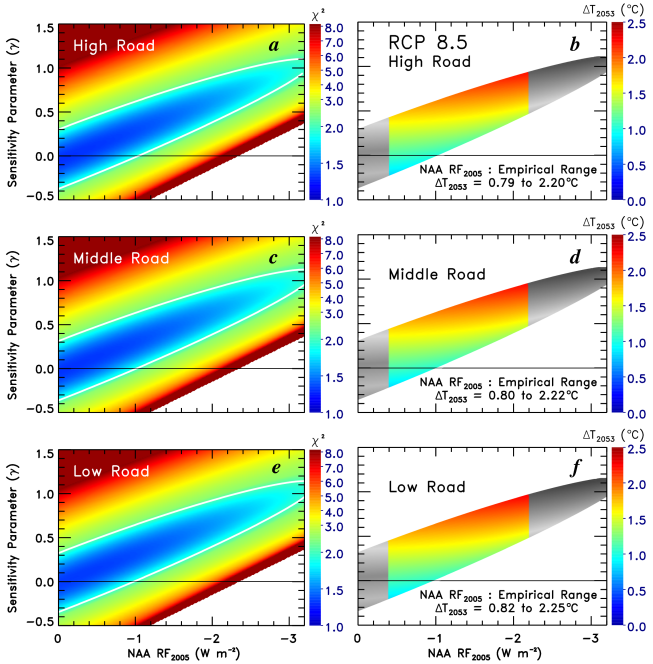

Fig. 7. Reduced chi-squared (χ^2) (left panels) and the global mean surface temperature anomaly in year 2053 (ΔT_{2053}) with respect to the 1961 to 1990 mean (right panels) as a function of sensitivity parameter γ and NAA RF_{2005}, for a simulation using GHG RF and NAA RF from RCP 8.5, constrained to match the OHC measurement of Church et al. (2011), for values of the scaling parameters α_{COOL} and α_{HEAT} along the High Road (panels **a** and **b**), Middle Road (panels **c** and **d**), and Low Road (panels **e** and **f**) of Fig. 4. The white contour on the left panels denotes $\chi^2 = 2$. Values of ΔT_{2053} are shown only for $\chi^2 \leq 2$ (i.e. only for acceptable fits to the climate record) and are depicted in color for regressions with NAA RF_{2005} between $-2.2\,W\,m^{-2}$ and $-0.4\,W\,m^{-2}$, the IPCC (2007)-based empirical range. The minimum and maximum values of ΔT_{2053} are noted.

ACPD
12, 23913–23974, 2012

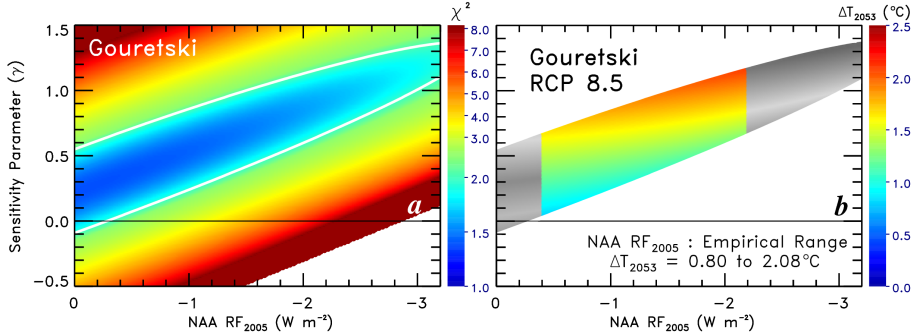

Fig. 8. Same as Fig. 7, except the model has been constrained to match OHC from Gouretski and Reseghetti (2010), for values of the scaling parameters α_{COOL} and α_{HEAT} along the Middle Road of Fig. 4.

ACPD
12, 23913–23974, 2012

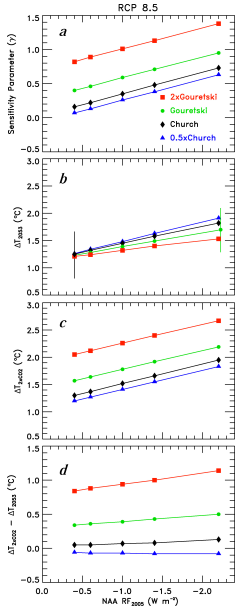

Fig. 9. Model parameters yielding best fits to the global, monthly mean CRU4 surface temperature anomaly, for regressions constrained by various values of NAA RF_{2005} and ocean heat content, for GHG and NAA RF from RCP 8.5. The regressions were conducted for five values of NAA RF_{2005}: the IPCC (2007)-based lower and upper empirical limits ($-2.2\,W\,m^{-2}$ and $-0.4\,W\,m^{-2}$), the IPCC (2007) best estimate ($-1.0\,W\,m^{-2}$), and the limits within 9 GCMs analyzed by Kiehl (2007) ($-1.4\,W\,m^{-2}$ and $-0.6\,W\,m^{-2}$). The different colors and symbols show results for various constraints on ocean heat content. Results are shown for OHC from: Church et al. (2011) (black ♦), Gouretski and Reseghetti (2010) (green •), 0.5×OHC from Church et al. (2011) (blue ▲), and 2×OHC of Gouretski and Reseghetti (2010) (red ■). Panel **(b)** includes error bars that reflect the range of ΔT_{2053} for acceptable fits, placed at the upper and lower limits of NAA RF_{2005}.

ACPD
12, 23913–23974, 2012

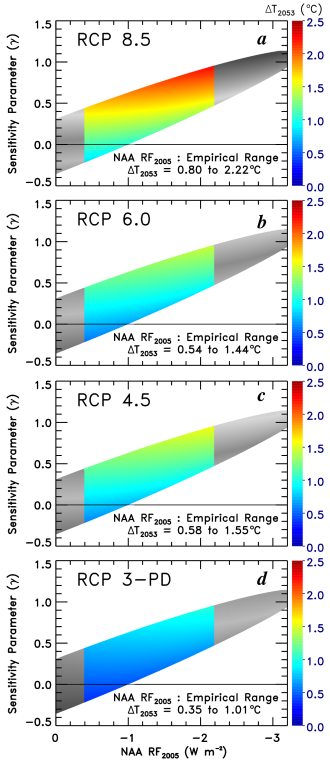

Fig. 10. ΔT_{2053} as a function of γ and NAA RF_{2005}, for GHG and NAA RF from the four RCP scenarios, as indicated. Model has been constrained to match OHC of Church et al. (2011).

ACPD
12, 23913–23974, 2012

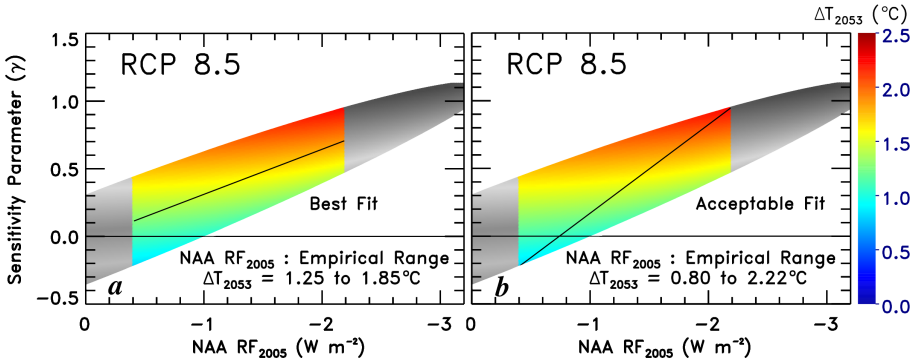

Fig. 11. ΔT_{2053} as a function of γ and NAA RF_{2005}, for GHG and NAA RF from RCP 8.5, constrained to match OHC of Church et al. (2011), together with lines indicating: **(a)** ΔT_{2053} versus NAA RF_{2005} based on best fit (minimum value of Cost Function) of the regression; **(b)** ΔT_{2053} versus NAA RF_{2005} based on acceptable fit ($\chi^2 \leq 2$) of the regression. For panel **(b)**, except for the extrema, there are multiple values of NAA RF_{2005} that could be associated with any particular value of ΔT_{2053}. We have chosen the depicted acceptable fit line so that the maximum range of ΔT_{2053} is represented. The range of possible values for ΔT_{2053}, given on each panel, expands considerably when acceptable fits are considered.

ACPD
12, 23913–23974, 2012

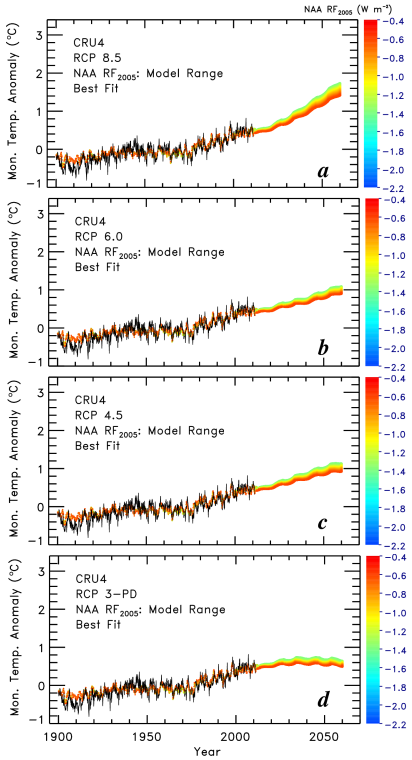

Fig. 12. ΔT as a function of time, for best fits to the regression, for calculations constrained by the Church et al. (2011) measurement of OHC, using GHG and NAA RF from the four RCP scenarios, as indicated. NAA RF_{2005} has been restricted to lie between $-1.4\,W\,m^{-2}$ and $-0.6\,W\,m^{-2}$, the GCM range reported by Kiehl (2007). The color bar showing values of NAA RF_{2005} associated with each value of ΔT can be taken literally, since for the best fit line there is a unique relation between future ΔT and NAA RF for the contemporary atmosphere, represented here as NAA RF_{2005}.

ACPD
12, 23913–23974, 2012

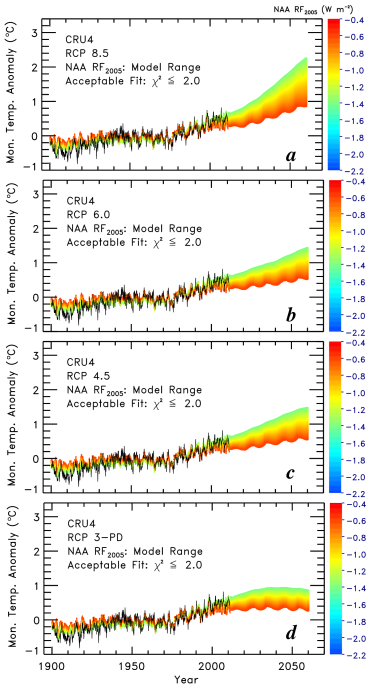

Fig. 13. Same as Fig. 12, except the range of possible values for ΔT_{2053} is based on a series of acceptable fit ($\chi^2 \leq 2$) lines such as the one depicted in Fig. 11b. The color bar showing values of NAA RF_{2005} is included, but this color bar represents only one possible way to sample the range of acceptable fits and should not be interpreted literally. Except for the extrema, there is not a unique relation between ΔT and NAA RF_{2005} for the set of acceptable fits. We have decided to include the color bar because it depicts the general sense of the relation between future temperature and NAA RF: i.e. the highest levels of future temperature are associated with acceptable fits to the historical temperature record that have large contemporary aerosol cooling and the lowest levels of future temperature are associated with fits having small contemporary aerosol cooling.

ACPD
12, 23913–23974, 2012

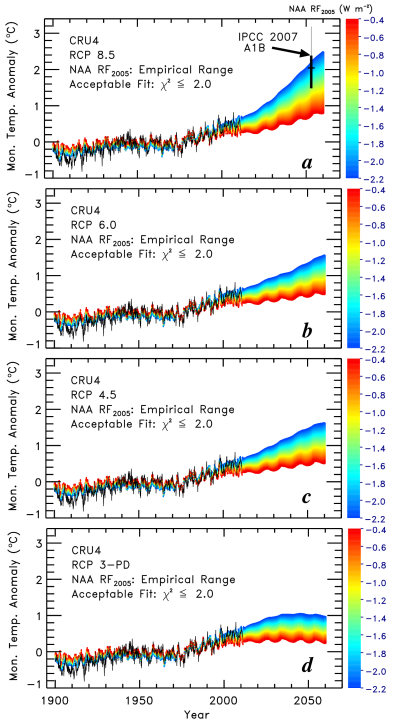

Fig. 14. Same as Fig. 13, except the range of NAA RF_{2005} has been expanded to $-2.2\,W\,m^{-2}$ and $-0.4\,W\,m^{-2}$, the IPCC (2007)-based empirical range. Panel **(a)** includes symbolic depiction of the GCM ensemble projection of ΔT from Fig. 10.5 of IPCC (2007), for the SRES A1B scenario. Atmospheric CO_2 is projected to double in 2053 according to RCP 8.5 and in 2060 according to SRES A1B. We have therefore placed the IPCC (2007) model results for year 2060 onto our figure at the time CO_2 will double according to RCP 8.5. We show the ensemble average (horizontal line), the range of 20 of the 21 ensemble members (thick line), and the outlier (thin line).

ACPD
12, 23913–23974, 2012

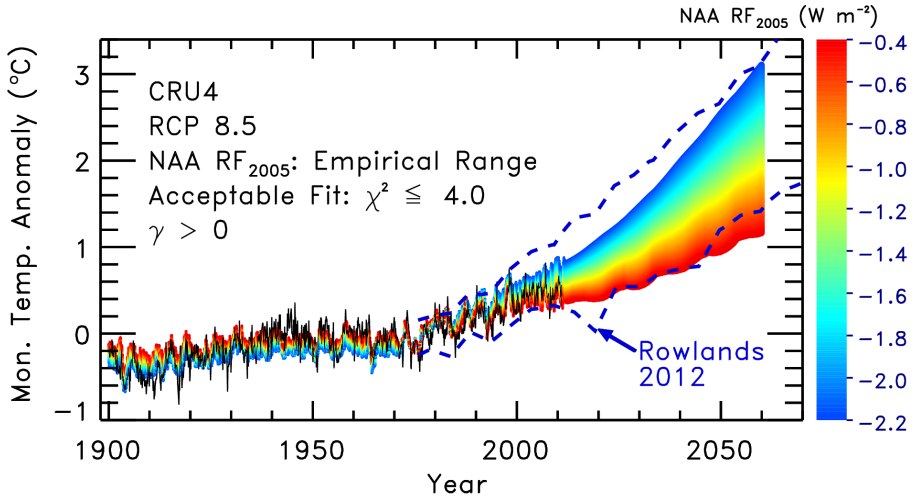

Fig. 15. Same as Fig. 14a, except the lines denote the "likely" range (66 % confidence interval) of a 9745 ensemble member set of GCM calculations constrained by SRES A1B that pass an acceptably test based on comparison to temperature observations over the 1961 to 2010 time period (Rowlands et al., 2012). The criteria for acceptable fit has been expanded to $\chi^2 \leq 4$ and $\gamma > 0$, so that the dispersion of ΔT generally matches the dispersion of ΔT from Rowlands et al. (2012).

ACPD
12, 23913–23974, 2012

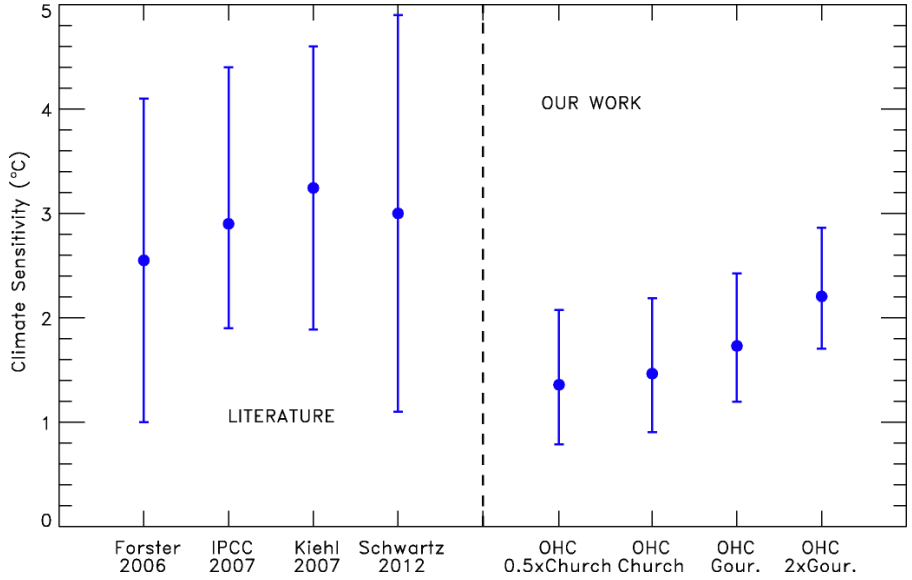

Fig. 16. Equilibrium climate sensitivity, $\Delta T_{2\times CO_2}$, from Forster and Gregory (2006), IPCC (2007), Kiehl (2007), and Schwartz (2007) (left half) compared to equilibrium climate sensitivity from our regressions, for fits to the OHC records of Church et al. (2011) and Gouretski and Reseghetti (2010), as well as 0.5× OHC of Church et al. (2011) and 2.0× OHC of Gouretski and Reseghetti (2010). The central point is for the best fit to NAA $RF_{2005} = -1.0\,W\,m^{-2}$ and the error bars represent the range of $\Delta T_{2\times CO_2}$, for the set of acceptable fits for the IPCC (2007)-based empirical range of NAA RF_{2005}. Numerical values of our climate sensitivities and ranges (i.e. points plotted), in units of °C, are 1.36 (+0.72, −0.57), 1.47 (+0.72, −0.56), 1.73 (+0.69, −0.53), and 2.20 (+0.66, −0.50) for the 0.5×Church, Church, Gour., and 2×Gour. measurements of OHC, respectively.

ACPD
12, 23913–23974, 2012

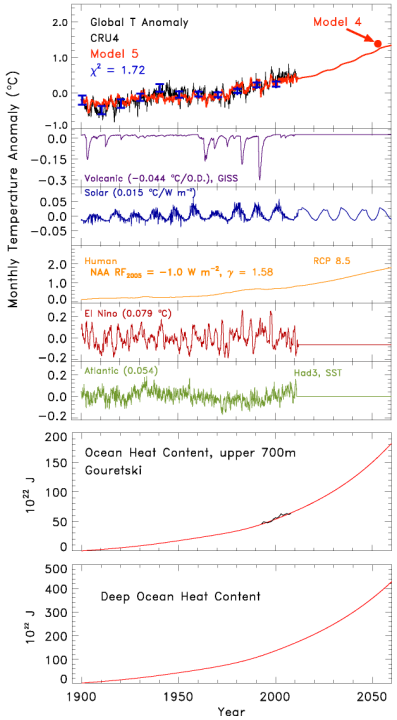

Fig. 17. Same as Fig. 6b, except the fraction of anthropogenic RF exported to the ocean, Ω, has been set to 0.72, resulting in a best fit value for γ of 1.6 (Model 5). This leads to $\Delta T_{2\times CO_2}$ = 2.9 °C, the IPCC (2007) best estimate of equilibrium climate sensitivity. The second to last rung of the ladder plot shows the measurement of OHC from Gouretski and Reseghetti (2010) compared to simulated OHC from Model 4 and the bottom rung of the ladder plot shows the difference between OHC from Model 5 and OHC from Model 4, which presumably must be exported to ocean depths below 700 m if Ω is truly as large as 0.7 and the Gouretski and Reseghetti (2010) determination of OHC is correct. The value of ΔT_{2053} from Model 5 (1.22 °C) is slightly smaller than the value from Model 4 (1.39 °C) (top rung).

ACPD
12, 23913–23974, 2012